The Environmental Influence on Tropical Cyclone Precipitation

EDWARD B. RODGERS

Laboratory for Atmospheres, NASA/Goddard Space Flight Center, Greenbelt, Maryland

JONG-JIN BAIK

Universities Space Research Association, Laboratory for Atmospheres, NASA/Goddard Space Flight Center, Greenbelt, Maryland

HAROLD F. PIERCE

SSAI, Lanham, Maryland

(Manuscript received 5 April 1993, in final form 31 October 1993)

ABSTRACT

The intensity, spatial, and temporal changes in precipitation were examined in three North Atlantic hurricanes during 1989 (Dean, Gabrielle, and Hugo) using precipitation estimates made from Special Sensor Microwave/Imager (SSM/I) measurements. In addition, analyses from a barotropic hurricane forecast model and the European Centre for Medium-Range Weather Forecast model were used to examine the relationship between the evolution of the precipitation in these tropical cyclones and external forcing. The external forcing parameters examined were 1) mean climatological sea surface temperatures, 2) vertical wind shear, 3) environmental tropospheric water vapor flux, and 4) upper-tropospheric eddy relative angular momentum flux convergence.

The analyses revealed that 1) the SSM/I precipitation estimates were able to delineate and monitor convective ring cycles similar to those observed with land-based and aircraft radar and in situ measurements; 2) tropical cyclone intensification was observed to occur when these convective rings propagated into the inner core of these systems (within 111 km of the center) and when the precipitation rates increased; 3) tropical cyclone weakening was observed to occur when these inner-core convective rings dissipated; 4) the inward propagation of the outer convective rings coincided with the dissipation of the inner convective rings when they came within 55 km of each other; 5) in regions with the combined warm sea surface temperatures (above 26°C) and low vertical wind shear (less than 5 m s^{-1}), convective rings outside the region of strong lower-tropospheric inertial stability could be initiated by strong surges of tropospheric moisture, while convective rings inside the region of strong lower-tropospheric inertial stability could be enhanced by upper-tropospheric eddy relative angular momentum flux convergence.

1. Introduction

The release of latent heat in deep convective cells provides the available potential energy necessary to maintain and intensify tropical cyclones (Palmén and Riehl 1957; and Riehl and Malkus 1961). The upward vertical motion in the deep convective cells causes subsidence-induced adiabatic warming in the eye that hydrostatically lowers the central pressure, increases the surface pressure gradient, strengthens the secondary circulation, and creates potential energy through the import of moisture and momentum into the system and mass out of the system. The organization of these deep convective cells into cyclonic bands helps to maintain the process of nonlinear cooperative interaction between the tropical cyclone scale and the cumulus scale (Ooyama 1964; Charney and Eliassen 1964). The local mass recycling (Gray and Shea 1973; Gray 1979) is also necessary for increasing surface energy flux that will enhance the release of latent heat.

The ability for the latent heat release (LHR) in these convective cells to intensify a tropical cyclone has been shown numerically to be greater as the tropical systems become more intense (Shapiro and Willoughby 1982; Delden 1989). Shapiro and Willoughby (1982) and Schubert and Hack (1982) suggested that the enhanced relationship between tropical cyclone diabatic heating and future intensification as the tropical system becomes more intense may be due to the positive nonlinear feedback process between increasing lower- and middle-tropospheric inertial stability and the increasing ability of the inner-core diabatic heating to warm the eye. They hypothesized that the more intense the tropical cyclone becomes, the greater the vortex circulation, lower- and middle-tropospheric inertial stability, secondary circulation, ascending motion in the eyewall,

Corresponding author address: Dr. Edward B. Rodgers, Mesoscale Dynamics and Precipitation Branch (Code 912), Laboratory for Atmospheres, NASA/Goddard Space Flight Center, Greenbelt, MD 20771.

and inner-core diabatic heating. The increase in the vortex circulation would, in turn, decrease the radius of the eye and, thereby, concentrate the compensating subsidence closer to the convective updrafts of the eyewall so that the adiabatic warming would become more intense. The enhanced warming within the eye would then hydrostatically lower the surface pressure, increase the pressure gradient and lower-tropospheric cyclonic tangential flow, accelerate the secondary circulation, and increase the potential energy of the system. The increase in the lower-tropospheric cyclonic tangential circulation will, in turn, increase the inertial stability and allow for greater warming, creating a positive feedback cycle.

Numerical model simulations (Kurihara and Tuleya 1974; Rosenthal 1978) and satellite infrared (Gentry et al. 1980; Steranka et al. 1986; Zehr 1988) and passive microwave (Adler and Rodgers 1977; Rodgers and Adler 1981; MacArthur 1991; Alliss et al. 1992) observations have demonstrated that the maximum increase of inner-core diabatic heating usually precedes tropical cyclone intensification. Numerical model simulations and satellite-flown infrared observational studies showed that the period of maximum LHR would precede the tropical cyclone maximum intensity by 24–72 h. The large variation in lag time is probably caused by the positive nonlinear feedback process between increasing efficiency of the inner-core diabatic heating and increasing lower- and middle-tropospheric inertial stability.

The changes of the organization of these convective precipitation bands also have a profound effect on the tropical cyclone intensity. Willoughby et al. (1982) and Willoughby (1988 and 1990) used research aircraft radar and in situ observations in conjunction with numerical models to identify a convective ring cycle. Convective rings, which contain annuli of intense axisymmetric cyclonic tangential winds and heavy convective precipitation, contract inward due to the LHR. The LHR in these rings causes subsidence in the enclosed area near the concentric ring, which produces adiabatic compressional warming, rapid isobaric height falls, and an increase in the gradient wind. In some intense hurricanes, outer convective rings may form around the inner eyewall, contract, and dissipate the convection in the inner eyewall through subsidence and the reduction of moisture inflow. The dissipation of the inner eyewall would end a period of tropical cyclone intensification and in some cases initiate a period of weakening. If, however, the outer convective ring continued to contract, the tropical cyclone would eventually reintensify. The large variation of tropical cyclone intensity may be caused by this convective ring cycle.

It appears from these studies that large temporal and spatial changes in tropical cyclone LHR are a precursor to tropical cyclone intensity change, particularly if the changes in diabatic heating occur near the center of circulation (Hack and Schubert 1986). Therefore, it is essential that the precipitation characteristics (e.g., rain intensity and distribution) in tropical cyclones are monitored. It is also important to better understand the process that controls the evolution of tropical cyclone precipitation.

Based on these earlier studies and the fact that tropical cyclones usually evolve over the oceans, where conventional data are scarce and not operationally available, it is apparent that satellite observations may aid in monitoring and increasing the understanding of the mechanisms that influence the tropical cyclone precipitation characteristics. Also, since the intensity in more mature systems may be altered by the large changes in diabatic heating, it may be possible to predict the subsequent intensity of a tropical cyclone if its precipitation characteristics are monitored by satellites.

This paper is intended to use satellite observations and operational numerical analyses to investigate the relationship between changes in tropical cyclone precipitation and intensity and the mechanisms that influence the variation of tropical cyclone precipitation. Three North Atlantic hurricanes were examined: Dean, Gabrielle, and Hugo (all in 1989). The hurricanes that were chosen remained primarily over the oceans during the months of August and September and had abundant Special Sensor Microwave/Imager (SSM/I) observations. Rain rates in these tropical cyclones were derived and monitored using the SSM/I on board the Defense Meteorological Satellite Program (DMSP) F-8. External environmental forcing mechanisms that may influence tropical cyclone precipitation were obtained from both the European Centre for Medium-Range Weather Forecasts (ECMWF) operational model (Shaw et al. 1987) and the barotropic hurricane track forecast model (VICBAR) (Ooyama 1987), while sea surface temperatures (SSTs) were obtained from climatological sea surface temperatures that were digitized on a 1° latitude × 1° longitude grid (Levitus 1982) and linearly interpolated to the position and time of each tropical cyclone.

2. External forcing mechanisms that may influence tropical cyclone precipitation

The changes in the precipitation of tropical cyclones over the oceans had been shown from earlier studies to be mainly controlled by various external forcing mechanisms such as sea surface moisture flux (a function of air and SSTs and surface winds) and radiational and environmental forcing. The SSTs have a profound influence on the tropical cyclone precipitation and intensity. For example, observational studies by Zehr (1992) have shown that tropical cyclogenesis in the western North Pacific never occurs when the SSTs are below 26°C. Further, theoretical and observational studies by Emanuel (1986) and Merrill (1988) have shown that the maximum intensity that a tropical cy-

clone can attain is limited by the SSTs. SSTs equal to and greater than 26°C allow for sufficient energy flux to support convection.

Radiational forcing may influence the precipitation in nondeveloping tropical clusters to cause a morning rainfall maximum and an afternoon minimum (Gray and Jacobson 1977). Geosynchronous flown infrared sensors were used to document similar diurnal variations in cloud-top temperatures in weak tropical cyclones (Steranka et al. 1984). These diurnal variations in cloud-top temperatures became less apparent as the tropical cyclone became more intense, however. Radiational forcing was found to be too weak compared to environmental forcing to maintain long-term variation in the cloud-top temperatures and rainfall, but could temporarily alter the convective trend depending on whether it is in phase with the environmental forcing.

The main environmental forcing mechanisms that have been documented to have a large influence on the variation of tropical cyclone precipitation are vertical wind shear, upper-tropospheric eddy relative angular momentum flux convergence (ERFC), and tropospheric water vapor flux. Strong vertical wind shear or strong upper-tropospheric ventilation would prevent the vertical alignment of the convective towers from occurring and would reduce the vertical transport of mass, moisture, and momentum that is necessary for tropical cyclone development (Gray 1979; Reuter and Yau 1986; Mundell 1991). The ability of the lower- and upper-tropospheric forcing to influence the precipitation within a tropical cyclone is mainly dependent upon the strength of the cyclonic tangential winds, however, and therefore, the magnitude of their inertial stability (Holland and Merrill 1984). Since the inertial stability of a tropical cyclone increases as the cyclonic tangential winds strengthen, the inertial stability becomes greater and more resistant to lateral displacement in the lower troposphere, particularly near the radius of maximum winds (Baik 1989) and weaker and less resistant to lateral displacement in the upper troposphere. Therefore, the inner- and outer-core precipitation in weak tropical cyclones should be influenced by both upper- and lower-tropospheric forcing. The inner-core precipitation that is located within the radius of maximum winds of an intense tropical system would probably be influenced by only the upper-tropospheric forcing, however.

The physical process that allows the lower-tropospheric forcing to alter the tropical cyclone precipitation within regions of weak lower-tropospheric inertial stability has been comparatively well documented and is believed to be related to surface evaporation (Frank 1977) and strong synoptic-scale low-level water vapor convergence (Ooyama 1964; Charney and Eliassen 1964; Molinari and Scubis 1985; Lee 1986). Water vapor budget studies within steady-state western North Pacific tropical cyclones (Frank 1977) indicated that water vapor convergence can contribute nearly 75% to the total precipitation at 222-km radius from their centers, however. At other radii, the water vapor convergence contributes less.

The physical mechanism by which the upper-tropospheric forcing alters the tropical cyclone precipitation in more intense tropical cyclones is less well understood. It has been demonstrated that the asymmetric outflow caused by the alignment of tropical cyclones with upper-tropospheric midlatitudinal, and tropical troughs (Sadler 1976, 1978) causes ERFC to occur (Pfeffer 1958; Palmén and Riehl 1957; Black and Anthes 1971; Holland 1983; Molinari and Vollaro 1989; Challa and Pfeffer 1980). The tropical cyclone precipitation, particularly near the center of circulation, could be enhanced by a gradient-wind adjustment process associated with the thermally direct circulation at the entrance region of the outflow jet (Merrill 1984; Shi et al. 1990; Rodgers et al. 1991) or by the ERFC-induced cyclonic spinup of the upper troposphere (Chen and Gray 1985; Rodgers et al. 1991).

Based on these studies, this paper will investigate how the variation of SSTs and the upper and lower troposphere alter the diabatic heating in these three tropical cyclones. To accomplish this task, variation in the tropical cyclone precipitation will be related to changes in SSTs, vertical shear, lower-tropospheric water vapor flux, and upper-tropospheric ERFC.

3. SSM/I-derived rain rates

a. SSM/I sensor

The SSM/I on board a DMSP satellite launched June 1987 measures microwave reflected and emitted radiation at frequencies of 19.4, 22.2, 37.0, and 85.5 GHz. The 22-GHz channel provides polarization only in the vertical, while the remaining channels are dual polarized. The SSM/I completes 14.1 revolutions per day along a near-sun-synchronous track at an altitude of 833 km. It scans conically at 45° from nadir and has an observational swath width of 1400 km at the earth's surface. Due to the orbit and narrow swath width, there is approximately a 90% probability that a tropical cyclone in the tropical regions will be observed at least once a day (Velden et al. 1989).

The brightness temperature T_B measured at SSM/I frequencies is a function of radiation emerging from the earth's surface and the state of the intervening atmosphere between the sensor and the earth's surface. The microwave energy emitted from the earth's surface at these frequencies is dependent on the earth's thermodynamic temperature and its emissivity, which varies according to the dielectric constant of the emitting surface. For example, a land area without vegetation that contains dry soil with low dieletric constant has high emissivity, and therefore, is characterized by high T_B, whereas a calm marine surface has a high dielectric constant, low emissivity, and therefore low T_B. An in-

crease in the surface winds over the ocean surface would increase the emissivity of the surface, however, thereby increasing the T_B.

Within the intervening atmosphere, the SSM/I T_B values are affected by the presence of molecular oxygen, atmospheric water vapor, liquid water droplets, and large ice particles, such as graupel or hail. Atmospheric water vapor and liquid water droplets radiate as blackbodies at their equilibrium temperature. Since their emissivity is greater than that of the water surfaces, but less than that of land surfaces, they radiate more than the ocean background but less than the land areas. Therefore, these constituents can be more easily observed over ocean areas by using these SSM/I channels. When the particle size of the large raindrops and ice become more comparable to the SSM/I wavelengths, scattering by these constituents becomes more pronounced. As a consequence, these large raindrops and ice particles scatter microwave radiation, thus lowering the T_B to values less than those observed over either land or water, and thereby making these constituents easier to be seen over both land and ocean surfaces.

b. *Brightness temperature–rain rate algorithm*

The algorithm used to estimate rain rate over the oceans from SSM/I-measured T_B's is described by Adler et al. (1993). The algorithm was chosen for its computational simplicity and because the rain rates were derived from the SSM/I's high spatial resolution channel. To derive rain rate from the SSM/I T_B's, the algorithm uses the horizontally polarized 85-GHz channel together with the 37-GHz horizontally polarized SSM/I channel. At these SSM/I frequencies, the surface is not seen when rain rates greater than 1 mm h^{-1} fill the instantaneous field of view (a high probability for a tropical cyclone). The 37-GHz channel defines raining areas over the ocean, while the 85 GHz defines rain intensity within the raining areas by measuring the ice scattering signature. The nonraining areas over the oceans were defined as regions where the 85-GHz T_B's minus the 37-GHz T_B's were greater than zero and the 37-GHz T_B's were less than 185 K. This raining–nonraining criterion over the oceans was based on a rain rate–T_B relationship developed from cloud model calculations (Adler et al. 1991). Over oceans where it rains, rain rates were determined from the 85-GHz T_B using a different rain rate–T_B relationship, also developed from the same cloud model. By using the 85-GHz SSM/I channel, the spatial distribution of the tropical cyclone rainbands is better resolved.

Huffman et al. (1993) evaluated the performance of the SSM/I rain-rate algorithm developed by Adler et al. (1993) over ocean regions by comparing the daily western Pacific atoll raingage measurements averaged for a given month with remotely observed mean monthly rain amounts obtained from both the SSM/I and the geosynchronous infrared (IR) (Adler and Negri 1993). Because of limited radar observations over the ocean, raingage measurements in the western Pacific were used as the "ground truth" instead. This evaluation, which took advantage of the better physical basis of microwave data and the better time resolution of geosynchronous IR data to estimate mean monthly rain amounts, emphasized the advantages of SSM/I characteristics. Results from this evaluation indicated that the rain amounts obtained remotely from satellites consistently underestimated the western Pacific atoll raingage measurements by a factor of 2. Because of this systematic underestimation of satellite-derived rain amounts, Huffman et al. (1993) increased the original SSM/I-derived rain rates over the ocean by a factor of 2. Since tropical cyclones occur predominantly over the ocean, the modified SSM/I algorithm (Huffman et al. 1993) was also used for this study.

c. *Sampling method*

To partition the retrieved SSM/I-derived rain rates into sectors, a "stereographic horizon grid" (Shenk et al. 1971) was first placed concentrically within each tropical cyclone center. The stereographic grid that was used in this study has eight annuli 55.5 km wide and eight azimuthal divisions. Retrieval rain rates were averaged for each sector. The center of the "stereographic horizon" map was placed at the center of the tropical cyclone and its zero azimuth line pointed north.

Figure 1 shows the geographically oriented "stereographic horizon" map superimposed upon the SSM/I-derived rain rates for Hurricane Hugo at 2110 UTC 15 September 1989. SSM/I-derived rain rates outside the "stereographic horizon" map were not sampled. The center of the stereographic horizon map was placed at the center of the circulation of Hurricane Hugo. The centers of circulation for Hugo, as well as the other two tropical cyclones that were studied, were based on the best-track data obtained from the 1989 Atlantic hurricane season report (Case and Mayfield 1990). The "stereographic horizon" map was used to sample the azimuthally averaged rain rates for eight annuli of 55-km width extending 444 km from the center of these tropical cyclones.

In addition to mean rain rates, LHR was calculated from the SSM/I using the rain-rate algorithm developed by Adler et al. (1993) and modified by Huffman et al. (1993). The areal LHR (W) is given by

$$\mathrm{LHR} = L\rho \int_A R\,da, \qquad (1)$$

where ρ (10^3 kg m^{-3}) is the density of the rainwater, L (2.5×10^6 J kg^{-1}) the latent heat of condensation, R (mm h^{-1}) the rain rate, da the incremental area, and A (m^2) the area of integration. Since earlier studies suggested that changes in the inner-core LHR were best related to subsequent changes in tropical cyclone in-

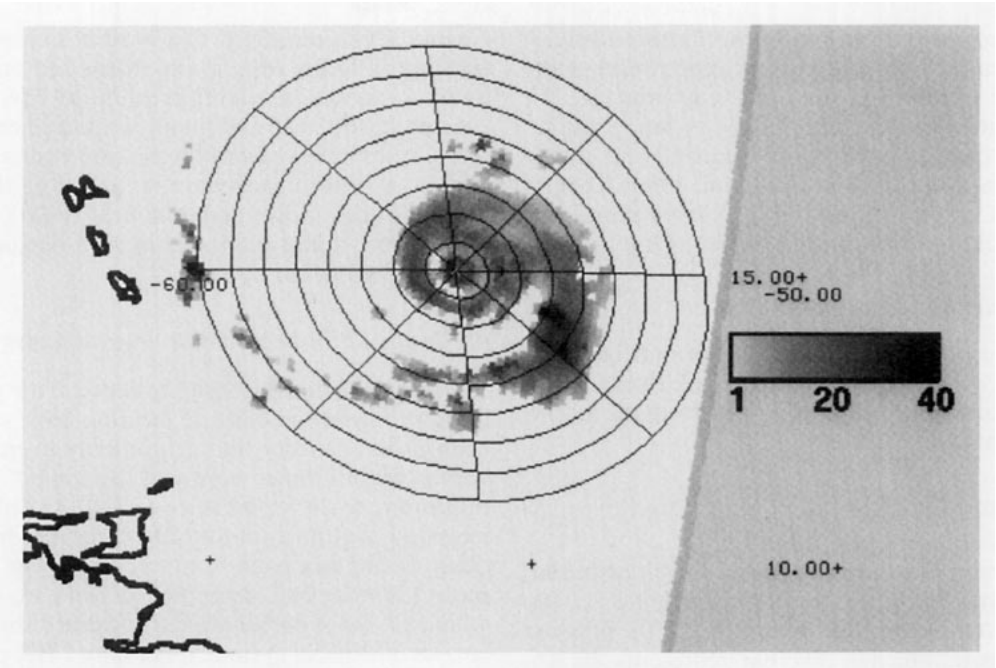

FIG. 1. SSM/I-derived rain rates (mm h^{-1}) for Hurricane Hugo at 2210 UTC 15 September 1989. Rain rates were sampled utilizing the stereographic horizon grid shown in the figure. The center of the grid is centered on Hugo's center of circulation and the annuli are 55 km in width. The light gray line traversing the grid depicts the edge of the SSM/I swath. White background denotes SSM/I-observed rain-free ocean background. Rain-rate amounts are delineated by the shaded wedge.

tensity, the integration of LHR was performed on the inner-core regions [within 111 km of the center (Weatherford 1987)] of these tropical cyclones.

4. Environmental diagnostics

The environmental diagnostic parameters used for this study were obtained from the ECMWF (Shaw et al. 1987) and VICBAR (Ooyama 1987) analyses. Both the VICBAR and ECMWF analyses were used to calculate vertical wind shear and upper-tropospheric ERFC (Demaria et al. 1993). Although the results for these parameters were similar, only the VICBAR-derived parameters are shown. The ECMWF analysis, on the other hand, was used to calculate tropospheric water vapor flux and to delineate the upper-tropospheric geopotential heights. The ECMWF (Reed et al. 1988) and VICBAR (Demaria et al. 1993) models were chosen for their ability to accurately analyze western Atlantic easterly waves and tropical cyclones. These diagnostic parameters were produced every 12 h (0000 and 1200 UTC) during each tropical cyclone day from the ECMWF and VICBAR analyses. The ECMWF analysis was archived on a 2.5° latitude × 2.5° longitude grid, while the VICBAR model was archived on a 1.0° latitude × 1.0° longitude grid.

a. Vertical shear

The vertical wind shear (m s^{-1}) within 500 km of the tropical cyclone was calculated from the 850- and 200-mb VICBAR wind analyses. The horizontal winds were averaged over the domain at the 850- and 200-mb level to derive a mean environmental wind vector at each level. The vertical shear was then estimated from the magnitude of the difference between the mean wind vectors at 850 and 200 mb.

b. Eddy RAM flux convergence

The upper-tropospheric ERFC (m s^{-1} day^{-1}) was calculated in Lagrangian cylindrical coordinates (Molinari and Vollaro 1989; Demaria et al. 1993) using the following equation:

$$\text{ERFC} = -\frac{1}{r^2}\frac{\partial}{\partial r}(r^2\overline{V_r'V_\theta'}), \qquad (2)$$

where r is the radius from the tropical cyclone center, V_r is the radial wind, and V_θ is the tangential wind. The overbar represents an azimuthal average and the prime denotes the deviation from the azimuthal average (e.g., eddy term). The radial and tangential winds in Langrangian coordinates were obtained from the 200-mb VICBAR and ECMWF wind analyses. The upper-tropospheric ERFC was calculated for an annulus whose inner and outer radii were, respectively, 600 and 1000 km from the tropical cyclone center. This annular area was used because it was comparable to the resolution of the VICAR and ECMWF analyses and because the satellite-derived upper-tropospheric wind observations used for these analyses were more

abundant outside the data-void central dense overcast region. When the tropical cyclone's upper-tropospheric anticyclonic outflow becomes more asymmetric, the ERFC becomes positive and thereby enhances the inner-core precipitation through a gradient wind adjustment process (Merrill 1984; Shi et al. 1990; Rodgers et al. 1991; Chen and Gray 1985). A more symmetric outflow would have an opposite effect.

c. *Areal mean horizontal moisture flux*

The tropospheric areal mean horizontal moisture flux (10^8 kg s^{-1}) was also calculated in Lagrangian cylindrical coordinate (Frank 1977) by using the following equation:

$$\text{moisture flux} = \frac{2\pi r}{g}\int_P \overline{V_r q}\,dp, \qquad (3)$$

where r is the radius from the tropical cyclone center, q is the mixing ratio, V_r is the radial wind, g is gravity, dp is the incremental pressure level, and P the pressure level of integration. The overbar represents an azimuthal average. The radial winds and mixing ratio were obtained from the 1000-, 850-, 700-, 500-, and 300-mb ECMWF analyses. The tropospheric moisture flux was calculated for cylindrical volume within 222 km of the center of circulation between 1000 and 300 mb. The cylindrical radius of 222 km was chosen for the following reasons: 1) the analysis was comparable to the resolution of the ECMWF analyses; 2) the lower- and middle-tropospheric wind observations were more abundant outside of the central dense overcast region; and 3) the water vapor budget studies that used the composite radiosonde data indicated that water vapor flux contributed more to the total precipitation within this circular area than surface evaporation (Frank 1977). Because of the inaccurate measurements of surface evaporation and the assumption that all water vapor convergence contributes to precipitation production, there was no attempt to relate the changes in the water vapor budget to changes in inner-core rain rate.

5. Tropical Cyclone Dean

Tropical Cyclone Dean (1–8 August 1989) was the first western North Atlantic hurricane examined in this study, and the weakest. Dean developed on a tropical wave that moved off the northwest coast of Africa on 27 July and slowly intensified to tropical storm stage on 1 August and to hurricane stage on 2 August. Dean continued to intensify with minimum surface pressure of 969 mb as it moved west-northwest. By 3 August, Dean slowed in forward speed and eventually curved northward on 5 August as the system moved toward a deepening upper-level western North Atlantic trough as seen from the ECMWF-derived 200-mb geopotential heights observed in Fig. 2. During the period of 4–6 August, Dean remained steady state as it accelerated northward. Dean, once again, intensified on 7 August to its minimum sea level pressure of 956 mb, then became steady state, and finally weakened on 8 August as the system moved northward into strong westerlies associated with a long-wave trough over the eastern United States (Case and Mayfield 1990). Figure 3 shows Dean's best track during 1–8 August and the SSM/I observation times.

a. *Dean's latent heat release versus intensity change*

To examine the relationship between the changes of Dean's inner-core diabatic heating and subsequent changes in intensity, the azimuthally averaged LHR within Dean's inner core was compared to Dean's minimum sea level pressure in Fig. 4. Although the temporal continuity of the SSM/I-derived mean LHR observations was poor, it appears from Fig. 4 that the mean LHR for the inner core reached a maximum on 4 August. Since earlier studies suggested that large increases in tropical cyclone inner-core LHR precede intensity change, it would be expected that this relationship would hold for the Dean case. This relationship, however, is not very obvious for Dean when the LHR is averaged over such a large area. Perhaps the reason why the relationship between Dean's inner-core diabatic heating and its future intensity change is weak is because Dean was a minimal hurricane and that the positive nonlinear feedback between diabatic heating and lower-tropospheric inertial stability was less. In order to better understand the relationship between changes in Dean's inner-core LHR and subsequent changes in the intensity, the evolution of the radial distribution of Dean's SSM/I-derived precipitation rates must be examined in better spatial resolution.

b. *The evolution of Dean's precipitation*

Figure 5, which shows the time change of the azimuthally averaged SSM/I derived rain rates for all eight annuli and the 12-h change in Dean's maximum surface winds, depicts a quantitative representation of the evolution of the radial distribution of Dean's SSM/I-derived precipitation rate. Although the SSM/I spatial and temporal coverage of Dean is poor, particularly on 2 August and in the outer annuli, the evolution of the rings with the heaviest precipitation rates can still be delineated. The rings that contain the heaviest precipitation rates will be defined as a convective ring following the work by Willoughby et al. (1982) and Willoughby (1988, 1990). This figure suggests that two convective rings formed and are denoted, respectively, by heavy dashed lines 1 and 2. The first convective ring was located within 55 km from Dean's center during 1–5 August. Precipitation rates in this convective ring were heaviest on 1 and 4

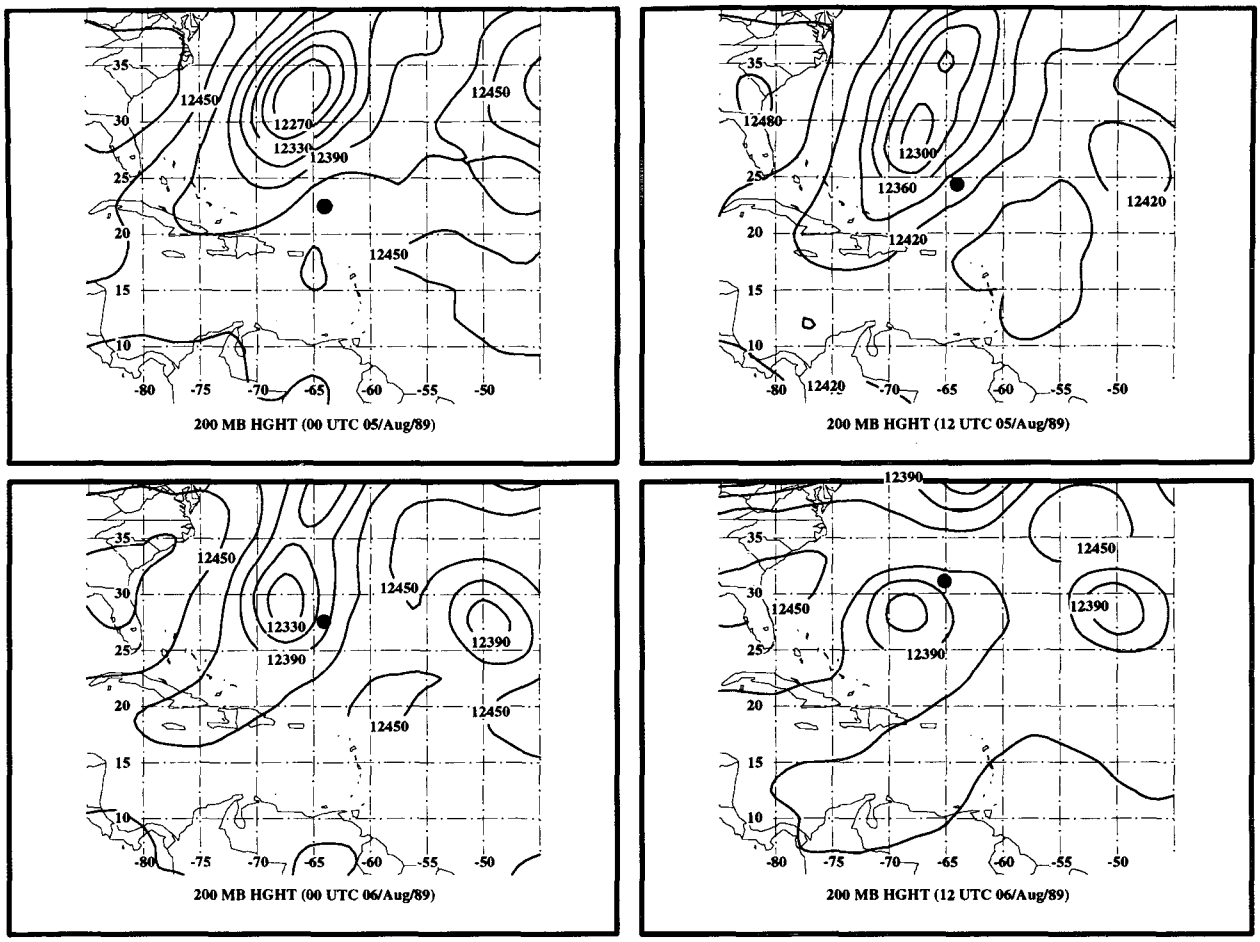

FIG. 2. ECMWF analysis of the western North Atlantic 200-mb geopotential heights (m) for 0000 and 1200 UTC for 5 and 6 August 1989. The dot represents Dean's best-track position at the given times.

August. On 4 August, the second convective ring was first observed at 277 km from the center, and propagated inward to within 111 km of the center on 6 August. Rain rates in the second convective ring were approximately one-half less than that observed in the first convective ring. On 5 August, as the second convective ring propagated inward, rain rates in the first convective ring decreased.

By comparing the evolution of these convective rings with Dean's maximum winds, the changes in mean precipitation rate in the first convective ring appeared to coincide with Dean's subsequent changes in intensity. The figure shows that Dean intensified on 2–4 August as the precipitation increased in the first convective ring. On 4 and 5 August, Dean's intensity became steady as the second convective ring formed, propagated inward, and dissipated the first convective ring. Dean reintensified on 6 August, as the second convective ring propagated further inward, but weakened on 7 August as the precipitation in the second convective ring decreased.

The evolution of Dean's convective rings appeared to be consistent with the convective ring cycle documented by Willoughby et al. (1982) and Willoughby (1988, 1990). For example, Dean's intensification appeared to coincide with the periods of enhanced precipitation in the first convective ring and the inward propagation of the second convective ring. On 3 August, Dean's intensity became steady when the precipitation in this convective ring decreased. The inward-propagating second convective ring enclosed the first convective ring and decreased the precipitation through subsidence and the reduction of moisture inflow (Willoughby et al. 1982; Willoughby 1988, 1990).

Thus, it appears from Fig. 5 that Dean's intensification episodes were associated with a convective ring cycle, which could not be detected by monitoring the azimuthally averaged LHR within the large inner-two annuli. The question that now needs to be answered is, What are the external forcing mechanisms that influence the initiation, maintenance, and dissipation of these convective rings?

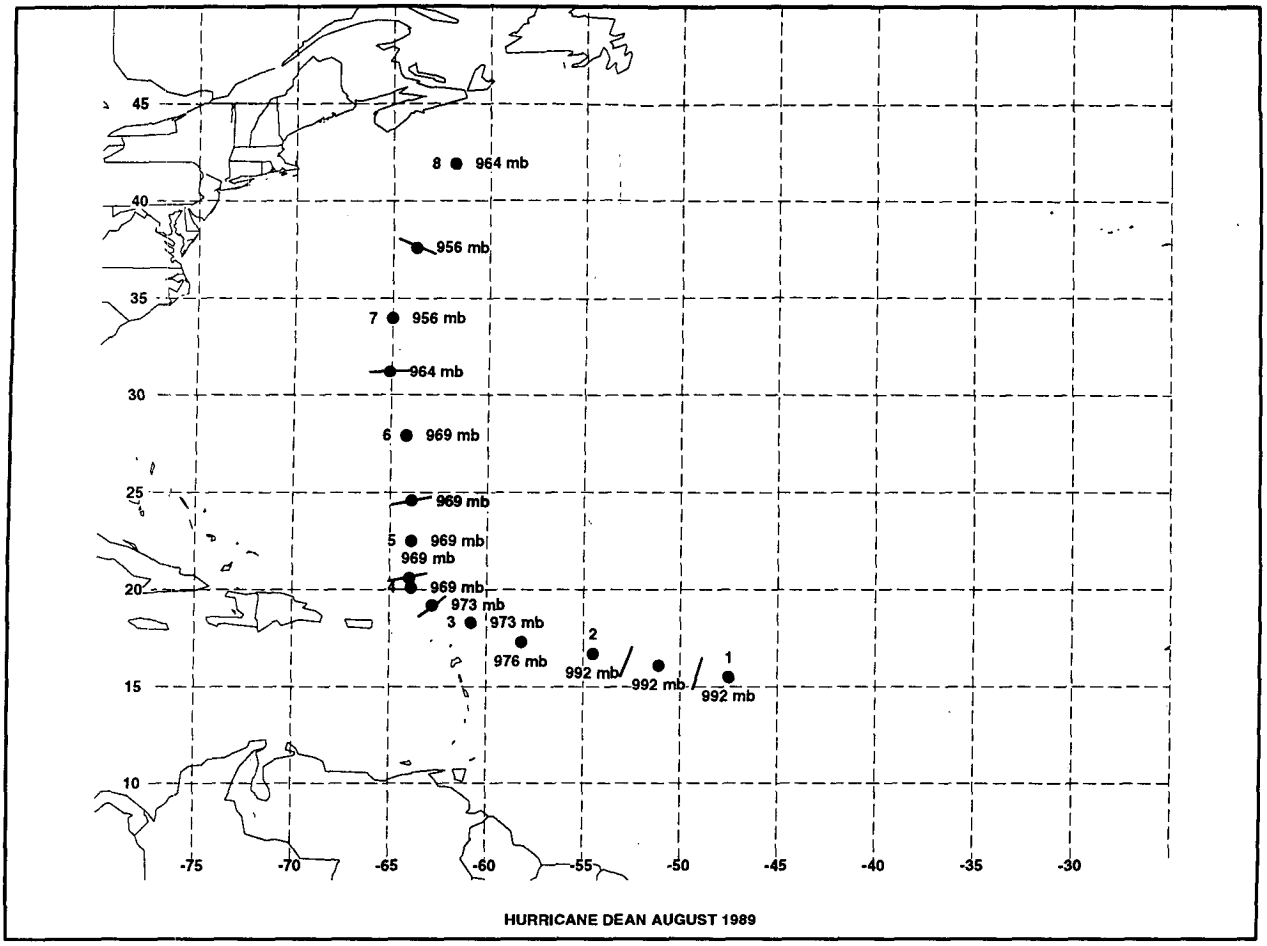

FIG. 3. The best-track positions and intensity (minimum central pressure in millibars) of western Atlantic Tropical Cyclone Dean (1–8 August 1989). Bars represent the approximate SSM/I observation times.

c. External influences on Dean's precipitation

Figure 6 shows the time change of Dean's SSM/I-derived azimuthal mean inner-core LHR (similar to LHR curve in Fig. 4) and the 12-h time change of Dean's external forcing parameters. Dean's external forcing mechanisms were related only to the azimuthally averaged LHR in the inner core, since LHR variations in this region of the tropical cyclone have the greatest effects on its subsequent changes in intensity (Schubert and Hack 1982). The figure shows the following:

1) The mean SSTs that Dean traversed increased to 28°C and then became steady until 6 August as Dean moved west and north. After 7 August, SSTs decreased abruptly to less than 20°C as Dean moved north of the Gulf Stream.

2) The vertical wind shear decreased on 2 August and then increased on 3 August and remained steady for nearly 24 h as Dean interacted with the first upper-level trough (Fig. 2). On 6 August, the vertical wind shear slowly decreased to a minimum as the first upper-tropospheric trough moved east of Dean and weakened, but increased once again as Dean interacted with the middle-latitudinal westerlies on 6 August.

3) On 2 August, a strong surge in the northeastern sector of the column caused an abrupt increase in the tropospheric water vapor flux on 2 August as Dean interacted with the first upper-tropospheric trough (Fig. 2), which reached a maximum early on 5 August. After 5 August, the water vapor flux decreased.

4) The upper-tropospheric ERFC remained less than 10 m s^{-1} day^{-1} until Dean interacted with the first upper-tropospheric trough (see Fig. 2). During the interaction with the first upper-tropospheric trough (Fig. 2) between 4 and 6 August, the ERFC increased, reaching its maximum on 6 August. As the first upper-level trough moved east of Dean and weakened, the ERFC decreased rapidly until 7 August. On 7 August, the ERFC increased, once again, as Dean began to interact with the westerlies.

Comparison between Figs. 5 and 4 shows that the changes of the azimuthally averaged LHR in Dean's

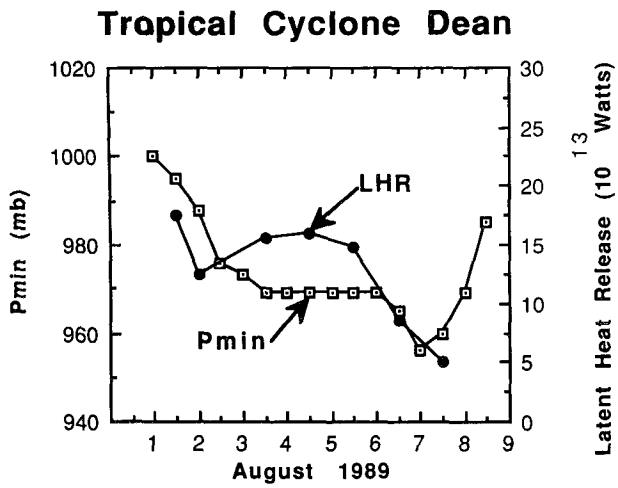

FIG. 4. A time plot of Dean's minimum central pressure (mb) and the SSM/I-derived azimuthally averaged latent heat release (10^{13} W) within the inner core (111 km of the center).

inner-core region were influenced by convective rings as they interacted with Dean's inner core. However, to better understand how external forcing influenced the evolution of these convective rings, we compared the mean precipitation rates in Fig. 5 to the external forcing parameters in Fig. 6.

Figures 5 and 6 suggest that the initiation and maintenance of the first convective ring between 1 and 2 August were caused by the increase in SSTs, the rapid decrease of vertical wind shear, and the slight enhancement of upper-tropospheric ERFC and tropospheric moisture flux. As SSTs remained high on 3 August, the decrease in the precipitation in this convective ring appeared to be related to the rapid increase in vertical wind shear. The ERFC once again increased as Dean began to interact with an upper-tropospheric trough on 4 August (Fig. 2). This increase in ERFC may have temporally enhanced the precipitation rates in this convective ring even though the vertical wind shear values remained moderately large (e.g., greater than 10 m s^{-1}).

The large increase in the inward flux of tropospheric water vapor that occurred between 3 and 4 August may also have enhanced the precipitation in the first convective ring. However, since Dean had reached minimum hurricane stage at this time and because the first convective ring was within 55 km of the center and near the radius of maximum winds, it is probable that Dean's high inertial stability prevented environmental tropospheric moisture from influencing the precipitation rates in this convective ring after 3 August. This large increase in the influx of tropospheric water vapor did appear to have a profound effect on the initiation of the second convective ring on 4 August, however. As the precipitation rates in the second convective ring increased, the adverse effect of the rapidly developing second convective ring that propagated inward helped to dissipate the first convective ring, even though the upper-tropospheric ERFC continued to increase after 4 August.

Since the second convective ring was outside the radius of maximum winds, the precipitation in this convective ring appeared to have been influenced by the inward surge of tropospheric moisture. For example, precipitation rates in the second convective ring reached a maximum on 5 August as troposphere moisture flux peaked. Also, the decreasing precipitation in this convective ring appeared to be linked to the rapid decrease in the inward flux of tropospheric water vapor that occurred after 5 August. As Dean moved north of the weakening upper-tropospheric trough (Fig. 2) after 6 August, both upper-tropospheric ERFC and vertical wind shear decreased. However, because of the rapidly decreasing influx of tropospheric moisture and cooler SSTs, precipitation decreased further. Finally, after 7 August, the second convective ring dissipated due to the combination of rapidly decreasing SSTs and

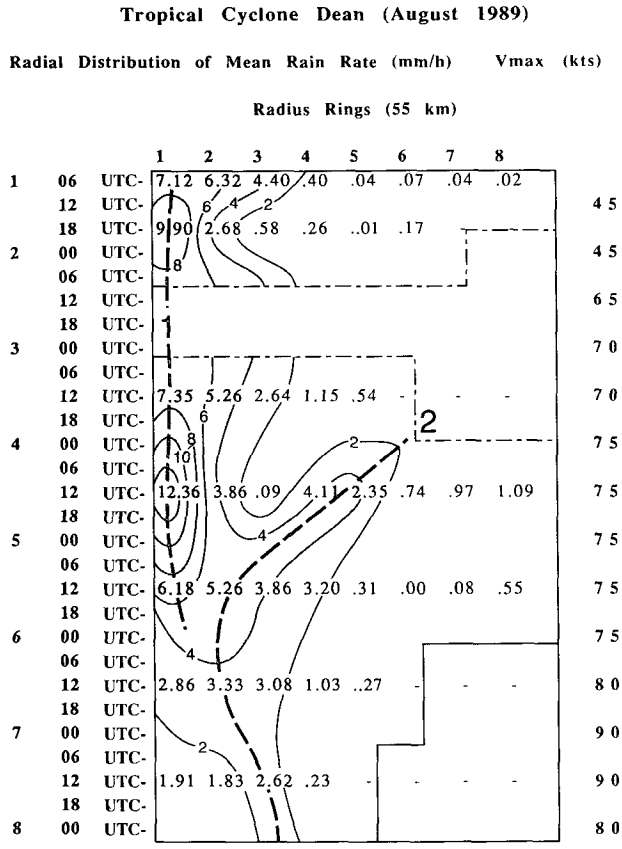

FIG. 5. The time change of Dean's azimuthally averaged SSM/I-derived rain rates (mm h^{-1}) for annuli 1–8 (55-km width) and maximum wind speed (kt) for Tropical Cyclone Dean. Contour intervals of rain rate are 2 mm h^{-1} and shaded regions delineate rain rates greater than 4 mm h^{-1}. The heavy dashed lines denote the axis with the heaviest rain rates, while the light dashed lines delineate regions with missing SSM/I observations.

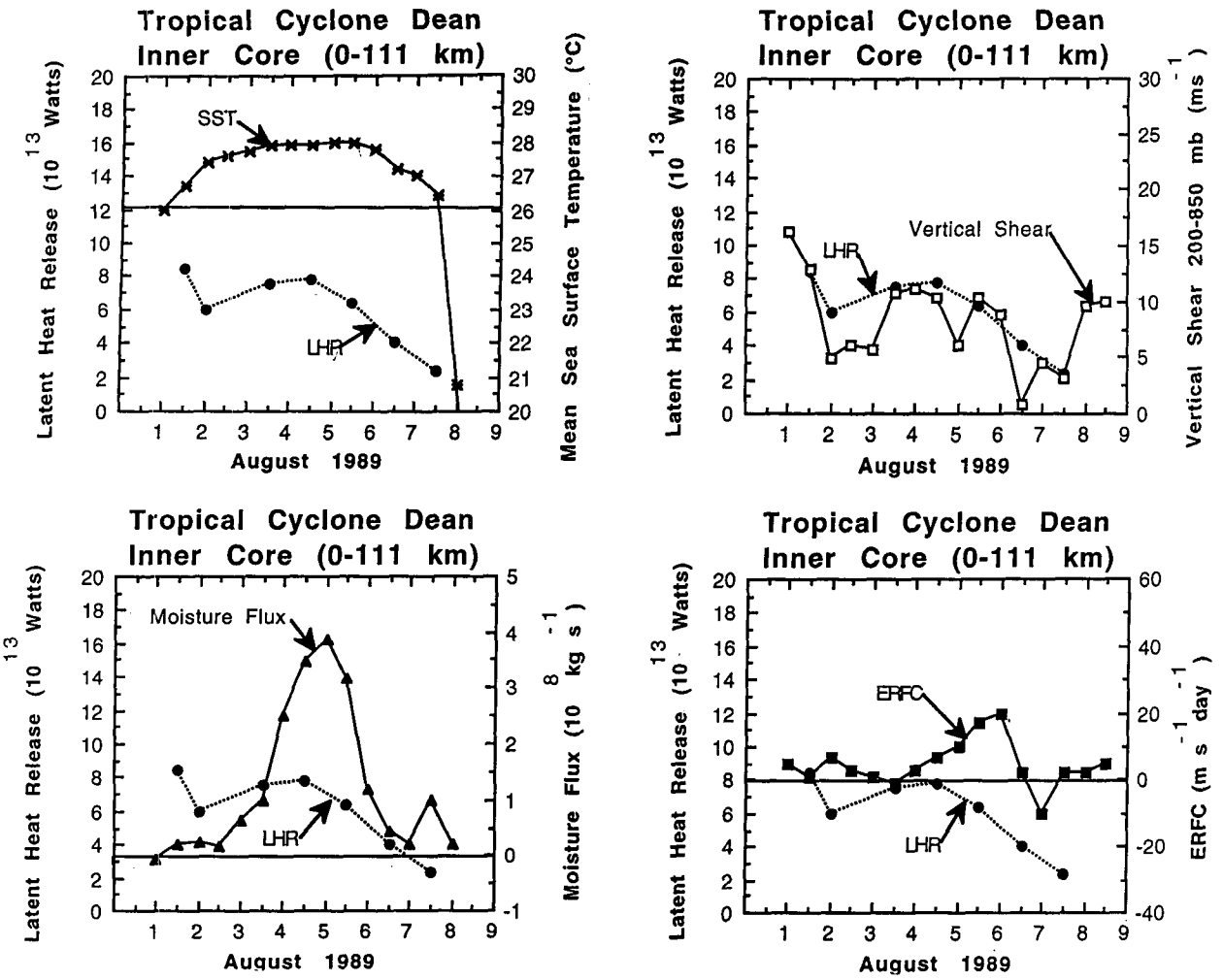

FIG. 6. A time plot of Dean's SSM/I-derived azimuthally averaged latent heat release (10^{13} W) within the inner core and the external forcing parameters. The external forcing parameters are sea surface temperatures (°C) in the upper-left panel, vertical wind shear (m s^{-1}) in the upper-right panel, tropospheric moisture flux (10^{8} kg s^{-1}) in the lower-left panel, and upper-tropospheric ERFC (m s^{-1} day^{-1}) in the lower-right panel.

strengthening vertical wind shear as Dean moved into the midlatitudinal westerlies.

Thus, it is apparent that the convective ring cycle (Willoughby et al. 1982; Willoughby 1988, 1990), played a major role in changing Dean's intensity and can be observed from SSM/I. It is also apparent that Dean's rain rates were greatly reduced in regions with high vertical wind shear and cool SSTs. On the other hand, in regions of warm SSTs and low vertical wind shear the influx of tropospheric moisture helped to initiate and maintain convective rings, particularly when the convective rings were outside the region of strong inertial stability, while Dean's upper-tropospheric ERFC enhanced precipitation in the inner-core convective rings. We will now examine Tropical Cyclones Gabrielle and Hugo to substantiate whether these findings are common for more intense tropical systems.

6. Tropical Cyclone Gabrielle

Gabrielle (1–11 September 1989) was more intense than Dean. Like Dean, Gabrielle also developed as an African wave. On 28 August, Gabrielle moved westward under the influence of the subtropical high to the north. Ideal upper-tropospheric ventilation allowed Gabrielle to rapidly develop to storm stage on 31 August and eventually to hurricane stage on 1 September. On 5 September, Gabrielle encountered an amplifying upper-tropospheric trough that caused the hurricane to recurve northward and intensify to a minimum surface pressure of 925 mb. The ECMWF-derived 200-mb geopotential heights (Fig. 7) depict the upper-tropospheric circulation pattern during this time. As Gabrielle continued northward between 9 and 11 September, the system slowed its forward motion, drifted westward, and weakened to tropical storm stage on 10

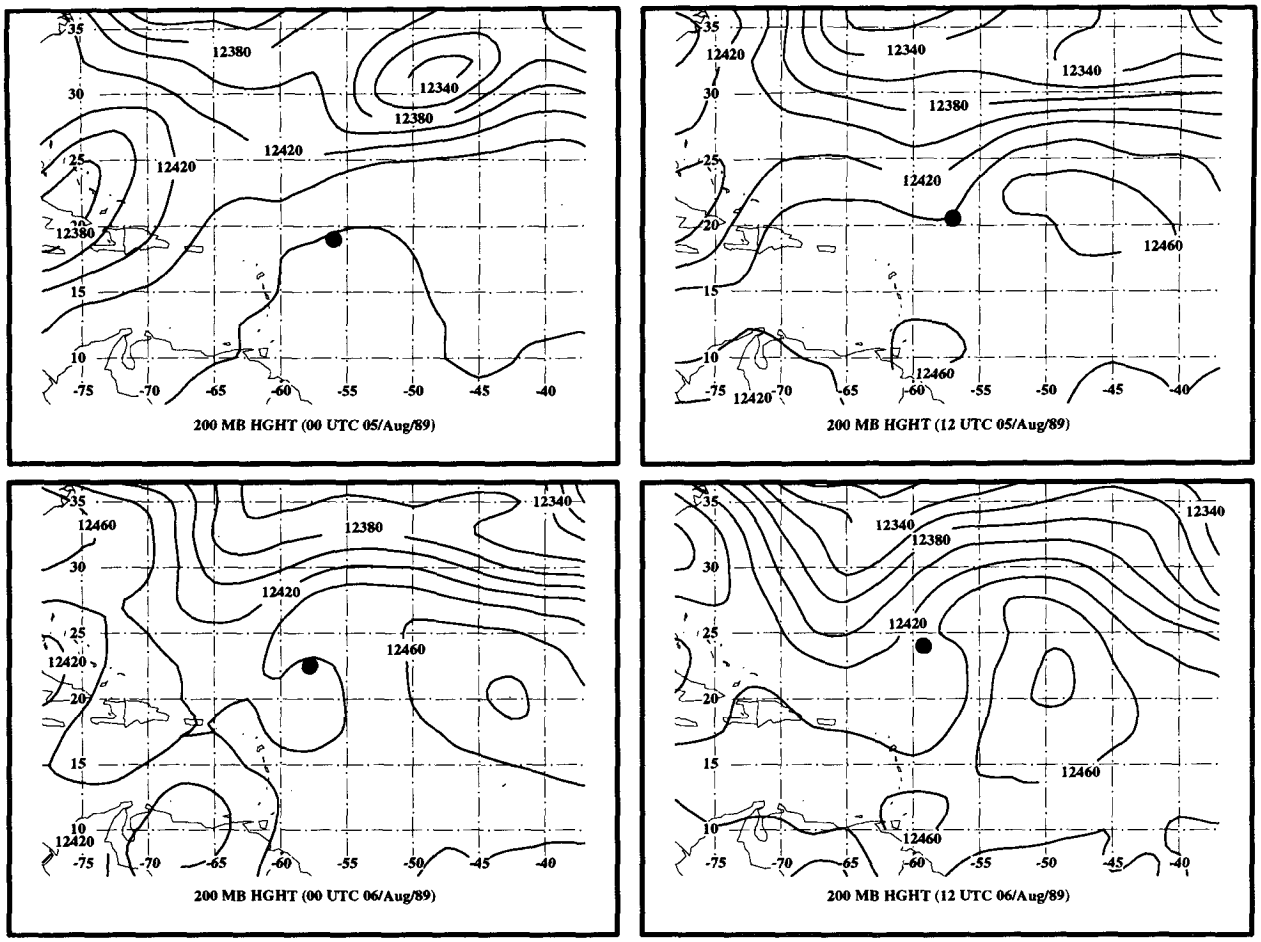

FIG. 7. ECMWF analysis of the western North Atlantic 200-mb geopotential heights (m) for 0000 and 1200 UTC for 5 and 6 September 1989. The dot represents Gabrielle's best-track position at the given times.

September as Gabrielle moved away from the influence of the upper-tropospheric trough. During most of Gabrielle's life, the system was large with hurricane-force winds extending out to 185 km from the center (Case and Mayfield 1990). Figure 8 shows Gabrielle's best track during 1–11 September and the SSM/I observation times.

a. Gabrielle's latent heat release change versus intensity change

The lag time between the mean inner-core LHR and subsequent changes in intensity as observed in Fig. 9 was more pronounced for Gabrielle than Dean, particularly during the hurricane stage. For example, large LHR amounts that occurred on 31 August and during 3–6 September, that were approximately two times greater than that observed in Dean, appeared to initiate and maintain Gabrielle's intensification. The decrease of inner-core LHR that occurred during 6–9 September, on the other hand, preceded the time when Gabrielle rapidly weakened.

b. The evolution of Gabrielle's precipitation

To better understand the relationship between the changes in Gabrielle's azimuthally averaged LHR and the system's subsequent intensity change, the evolution of the radial distribution of Gabrielle's SSM/I-derived precipitation rates and intensity is shown in Fig. 10. The figure clearly depicts convective ring cycles (Willoughby et al. 1982; Willoughby 1988, 1990) similar to those observed with Tropical Cyclone Dean. Although the temporal and spatial coverage of SSM/I is poor, the sensor is still able to delineate three convective rings (denoted, respectively, by heavy dashed lines 1, 2, and 3). The first convective ring originated at 165 km from the center early on 31 August, propagated inward, and dissipated on 3 September. Precipitation in this convective ring decreased between 1 and 2 September, but increased, once again, on 3 September. The second convective ring originated at 165 km from the center late on 2 August and propagated inward to within 111 km of the center. After Gabrielle recurved northward on 5 September, precipitation increased to

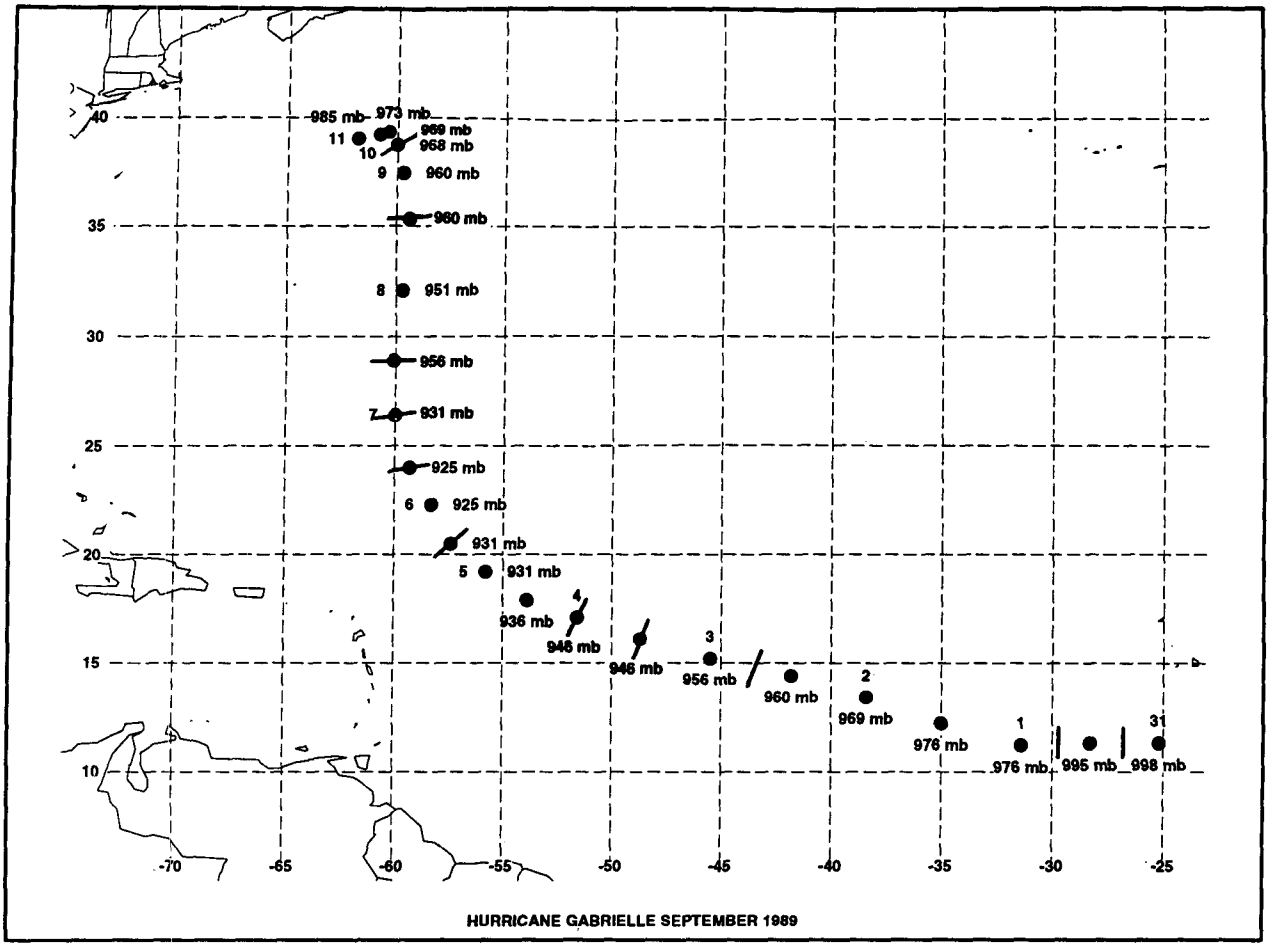

FIG. 8. The best-track positions and intensity (minimum central pressure in millibars) of western Atlantic Tropical Cyclone Gabrielle (1–11 September 1989). Otherwise, similar to Fig. 3.

a maximum value of nearly 12 mm h^{-1}. As the convective ring moved to within 55 km of the first convective ring, the first convective ring appeared to dissipate. The third, and the weakest, of the convective rings appeared on 6 September between 222 and 277 km from the center and quickly dissipated on 8 September. This convective ring may have aided in the dissipation of the second convective ring as Gabrielle weakened.

It is noted from the plan view of Gabrielle's SSM/I-derived rain rates for 0954 UTC 6 September (Fig. 11) that the southwestern sector of the system was nearly void of precipitation. Gabrielle maintained this asymmetry in its precipitation pattern during its northward movement. As the system continued to move northward, precipitation rates decreased further.

The comparison between the evolution of Gabrielle's radial distribution of the SSM/I-derived azimuthally averaged precipitation rates and maximum winds (Fig. 10) shows that Gabrielle rapidly intensified during the period between 31 August and 3 September as the first convective ring propagated inward. On 4 September, as the second convective ring formed, propagated inward, and caused the first convective ring to dissipate, Gabrielle intensified more slowly. On 5 September, as the second convective band propagated inward and the precipitation rates increased, Gabrielle's intensity became steady. Unlike the first convective ring, however, the second convective ring never reached the annulus nearest to the center (i.e., 55-km distance from the center). On 6 September, Gabrielle continued to intensify and reached its maximum intensity approximately 12 h after the maximum precipitation rates occurred in this convective ring. After 6 August, the formation of the third convective ring, which appeared to help reduce the rain rates in the second convective ring, marked the final weakening phase of Hurricane Gabrielle.

Thus, it appears from the evolution of Gabrielle's radial distribution of precipitation rates that the SSM/I was able to observe convective ring cycles, just as in Tropical Cyclone Dean. The convective ring cycles

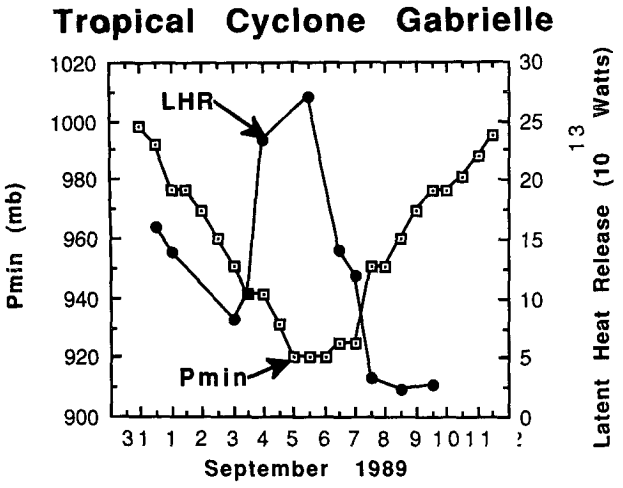

FIG. 9. A time plot of Gabrielle's minimum central pressure and the SSM/I-derived inner-core azimuthally averaged latent heat release. Otherwise, similar to Fig. 4.

were different from those observed with Dean, however. For example, Gabrielle had three convective ring cycles rather than two and the duration of Gabrielle's second convective ring was longer than either of Dean's convective ring cycles. Although Gabrielle was more intense than Dean, Gabrielle's convective rings were located farther from the center.

c. *External influences on Gabrielle's precipitation*

Figure 12 shows the external forcing mechanisms that may have influenced Gabrielle's convective ring cycles. Comparison between the inner-core azimuthally averaged LHR with Gabrielle's external forcing parameters indicates that:

1) The SSTs that Gabrielle encountered decreased to 26.5°C on 2 September and than began to increase slowly to a maximum value of 28°C on 6 September. After 6 September, SSTs quickly decreased as Gabrielle moved north of the Gulf Stream.

2) Strong vertical wind shear (e.g., greater than 10 m s^{-1}) that occurred from 31 August through 2 September decreased to values less than 5 m s^{-1} on 3 September. After 3 September, vertical wind shear increased slowly, reaching a maximum on 8 September as Gabrielle interacted with the upper-tropospheric trough (Fig. 7), but weakened once again as Gabrielle moved away from the upper-tropospheric trough.

3) The inward flux of tropospheric moisture decreased during 1 September and became negative on 2 September. As Gabrielle began to recurve northward, the inward flux of moisture increased during the following day and became positive between 3 and 4 September. After 5 September, a second inward surge of moisture occurred, which increased the flux to maximum values of more than 5×10^8 kg s^{-1} between 7 and 8 September as Gabrielle intensified and the moisture flux at 222 km from the center came under the influence of Gabrielle's large circulation. After 8 September, as Gabrielle rapidly weakened, the influx of tropospheric moisture decreased. The azimuthally measured tropospheric water vapor flux indicated that during the period between 6 and 9 September the large increase in the inward flux of tropospheric moisture observed in Fig. 12 was caused by a large moisture surge in the northern sector of Gabrielle as the system accelerated northward. On the other hand, the large outward flux of moisture in the southern sector of Gabrielle probably aided in decreasing the precipitation rates in this region as seen Fig. 11.

4) From 31 August to 9 September, the upper-tropospheric EFRC increased slowly from negative values before 2 September to a maximum on 9 September as Gabrielle began to interact with the upper-tropospheric trough (see Fig. 7). Maximum values were approximately two times larger than those found in Hurricane Dean. After 9 September, upper-tropospheric ERFC

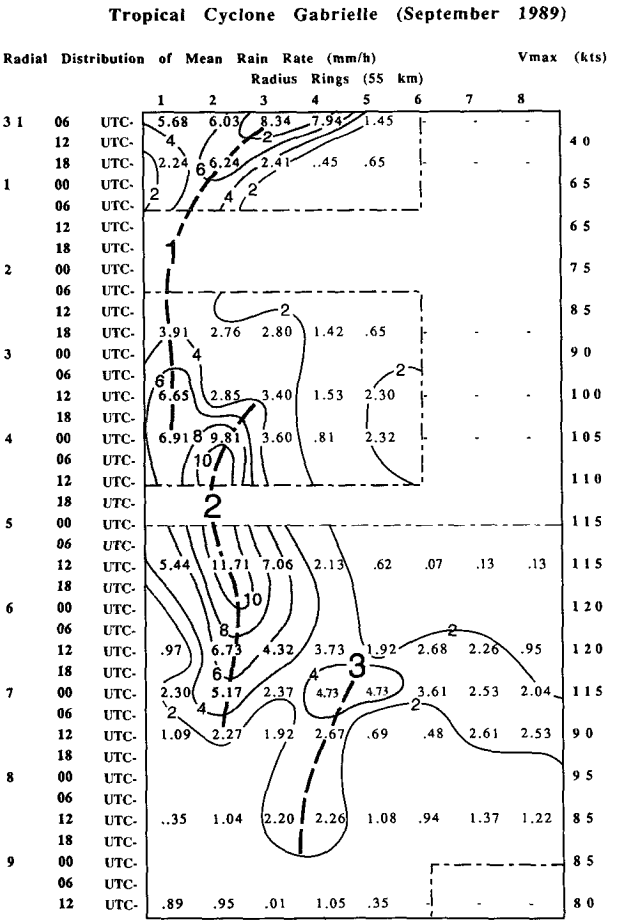

FIG. 10. The time change of Gabrielle's azimuthally averaged SSM/I-derived rain rates for annuli 1–8 and maximum wind speed. Otherwise, similar to Fig. 5.

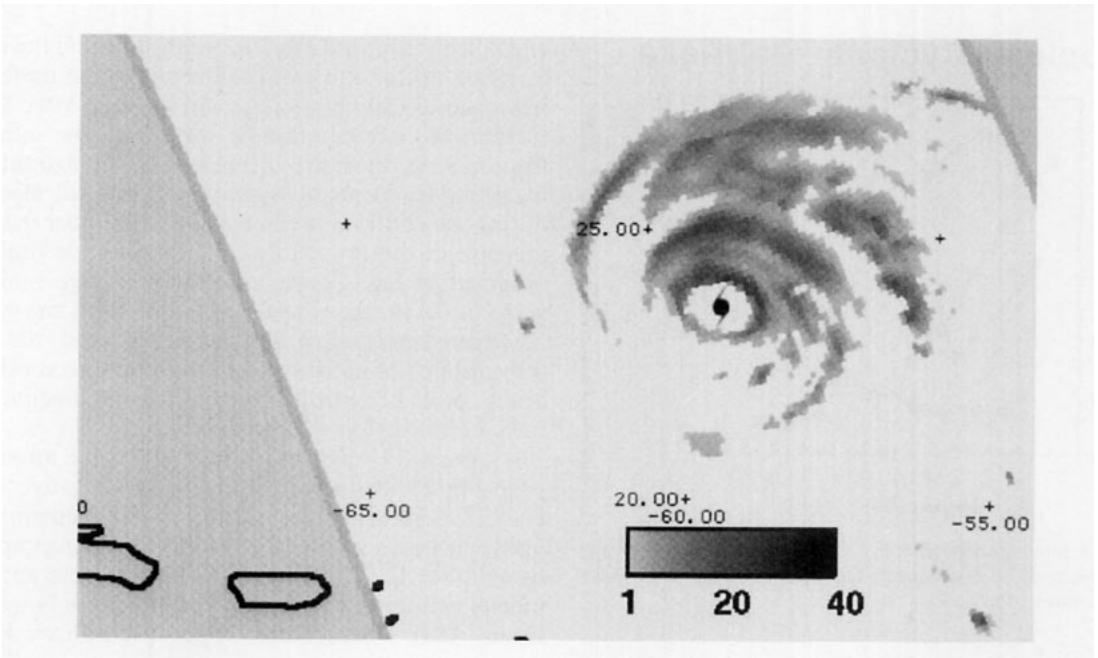

FIG. 11. SSM/I-derived rain rates (mm h^{-1}) for Hurricane Gabrielle at 0954 UTC 6 September 1989. The hurricane symbol represents the center of the tropical cyclone. Otherwise, similar to Fig. 1.

abruptly decreased to negative values as the upper-tropospheric trough propagated southward away from Gabrielle.

By comparing Fig. 10 with Fig. 9, it is apparent that the changes of the azimuthally averaged LHR in Gabrielle's inner-core region were influenced by the three convective rings as they interacted with Gabrielle's inner core. To understand how external forcing influenced the evolution of these convective rings, however, the mean precipitation rates in Fig. 10 were compared to the external forcing mechanisms in Fig. 12.

It is seen from the comparison of Figs. 10 and 12 that the maintenance of the first convective ring (31 August through 1 September) that is located 165 km from the center appeared to occur as Gabrielle encountered warm SSTs (>27°C) and an influx of tropospheric moisture. However, decreasing precipitation rates that occurred between 1 and 2 September coincided with the loss of tropospheric water vapor flux, strong vertical wind shear (>10 m s^{-1}), and decreasing SSTs as the convective ring propagated inward. On 3 September, rain rates increased, once again, as SSTs and upper-tropospheric ERFC increased and vertical shear rapidly decreased. Although the influx of tropospheric water vapor was increasing rapidly at this time, the weak influx of water vapor probably did not reach the convective ring due to strong lower-tropospheric inertial stability associated with Hurricane Gabrielle.

Outside the radius of maximum winds where the inertial stability was weaker, however, the tropospheric inward flux of moisture on 3 September may have aided in initiating the second convective ring. The second convective ring probably dissipated the first convective ring by reducing the inward flux of moisture and subjecting the inner convective ring to upper-tropospheric subsidence. Since the second convective ring was further from the center than the first and the lower-tropospheric inertial stability was weaker in this region, the increase in the precipitation rates in the second convective ring on 5 September may have been caused by the increased influx of tropospheric moisture as the system encountered warm SSTs and low vertical wind shear.

On 6 September, as Gabrielle recurved more northward, the rapid increase in the lower-tropospheric moisture flux appeared to coincide with the initiation of Gabrielle's third convective ring. The inward propagation of the third convective ring probably dissipated the second convective ring, even though SSTs and upper-tropospheric ERFC continued to increase and the vertical wind shear remained weak. Although the upper-tropospheric ERFC and lower-tropospheric moisture flux continued to increase after 7 September, it appears that the rapidly cooling SSTs and increasing vertical wind shear reduced the precipitation in the third convective ring as Gabrielle moved further northward.

Thus, it is apparent that the convective ring cycle can be monitored from SSM/I and that these convective rings played a major role in changing Gabrielle's intensity. It was also apparent that Gabrielle's rain rates were greatly reduced in regions with high vertical wind shear and cool SSTs. In regions of warm SSTs and low vertical wind shear, however, tropospheric moisture

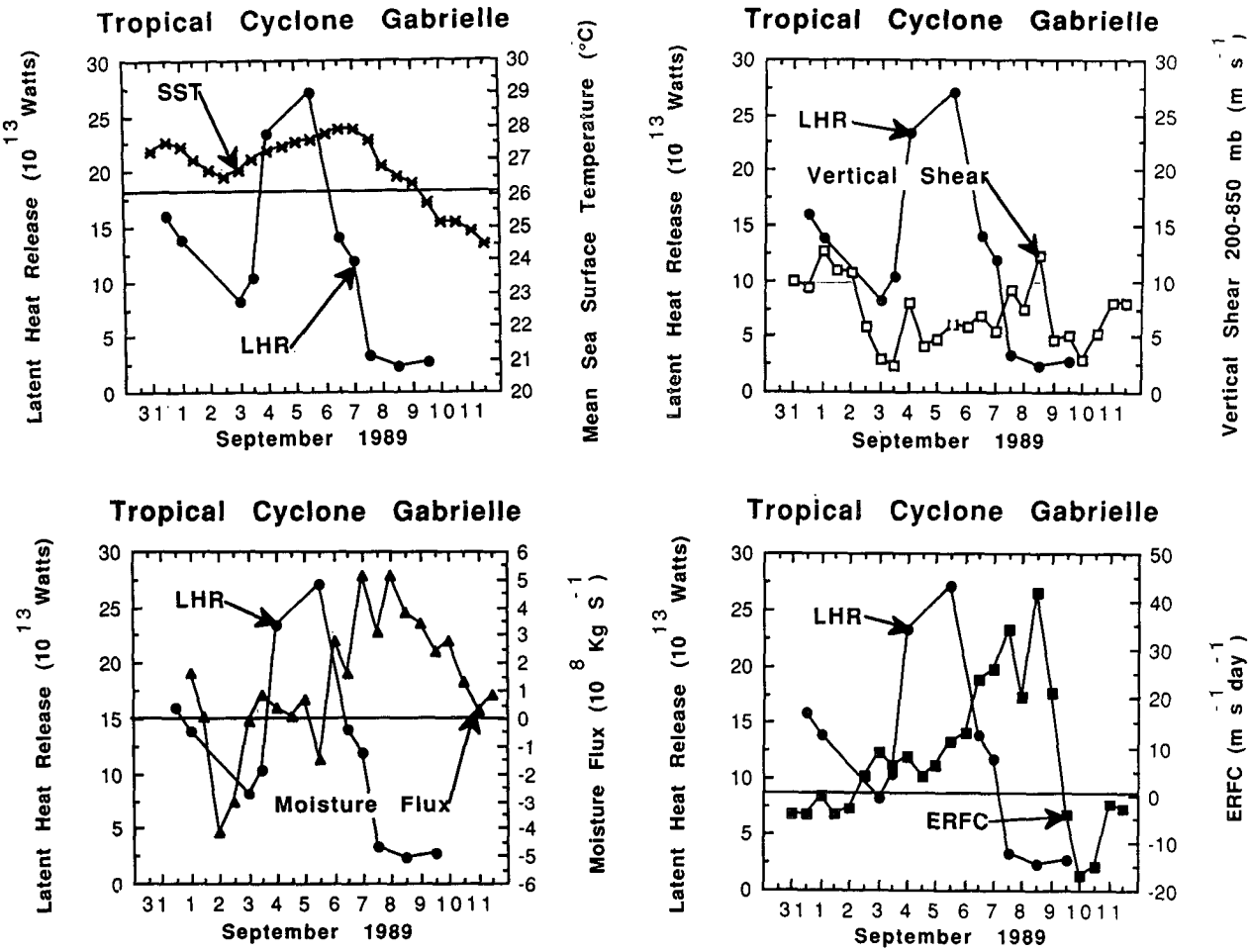

FIG. 12. A time plot of Gabrielle's inner-core SSM/I-derived azimuthally averaged latent heat release and the external forcing parameters. Otherwise, similar to Fig. 6.

flux helped to initiate and maintain the convective rings at all radii when the system was weak and the convective rings outside of the radius of maximum winds when the system was at hurricane stage. The upper-tropospheric ERFC, on the other hand, had a minor effect on Gabrielle's precipitation rates. Perhaps the strong vertical wind shear that Gabrielle encountered after 6 September when the system interacted with the upper-tropospheric trough masked the forcing that was caused by the strong upper-tropospheric ERFC during this time. To further substantiate whether these findings are common for the more intense tropical cyclones, however, Tropical Cyclone Hugo will now be examined.

7. Tropical Cyclone Hugo

The third system that was examined, and by far the most intense of the three, was Tropical Cyclone Hugo (10–22 September 1989). Like Dean and Gabrielle, Hugo developed off the African coast and moved westward. The system intensified rapidly and became a tropical storm on 11 September and a hurricane on 13 September. As Hugo approached the Leeward Islands, the system slowed in forward speed, turned to the west-northwest, and continued to intensify. On 16 September, Hugo reached its maximum intensity, with a central sea level pressure of 910 mb, as it continued to decelerate. Hugo passed directly over the island of Guadeloupe on 17 September and St. Croix on 18 September. Later that day, as Hugo accelerated, once again, the system moved over the eastern tip of Puerto Rico. Subsequently, Hugo rapidly weakened and turned more northward. As Hugo moved further northwestward on 20 September, the system's motion became influenced by a subtropical upper-tropospheric ridge to the northeast and an upper-tropospheric closed low to the southwest. These two synoptic-scale upper-tropospheric systems helped to reintensify and accelerate Hugo toward the South Carolina coast. The ECMWF 200-mb geopotential heights in Fig. 13 depict the upper-tropospheric circulation pattern during this time.

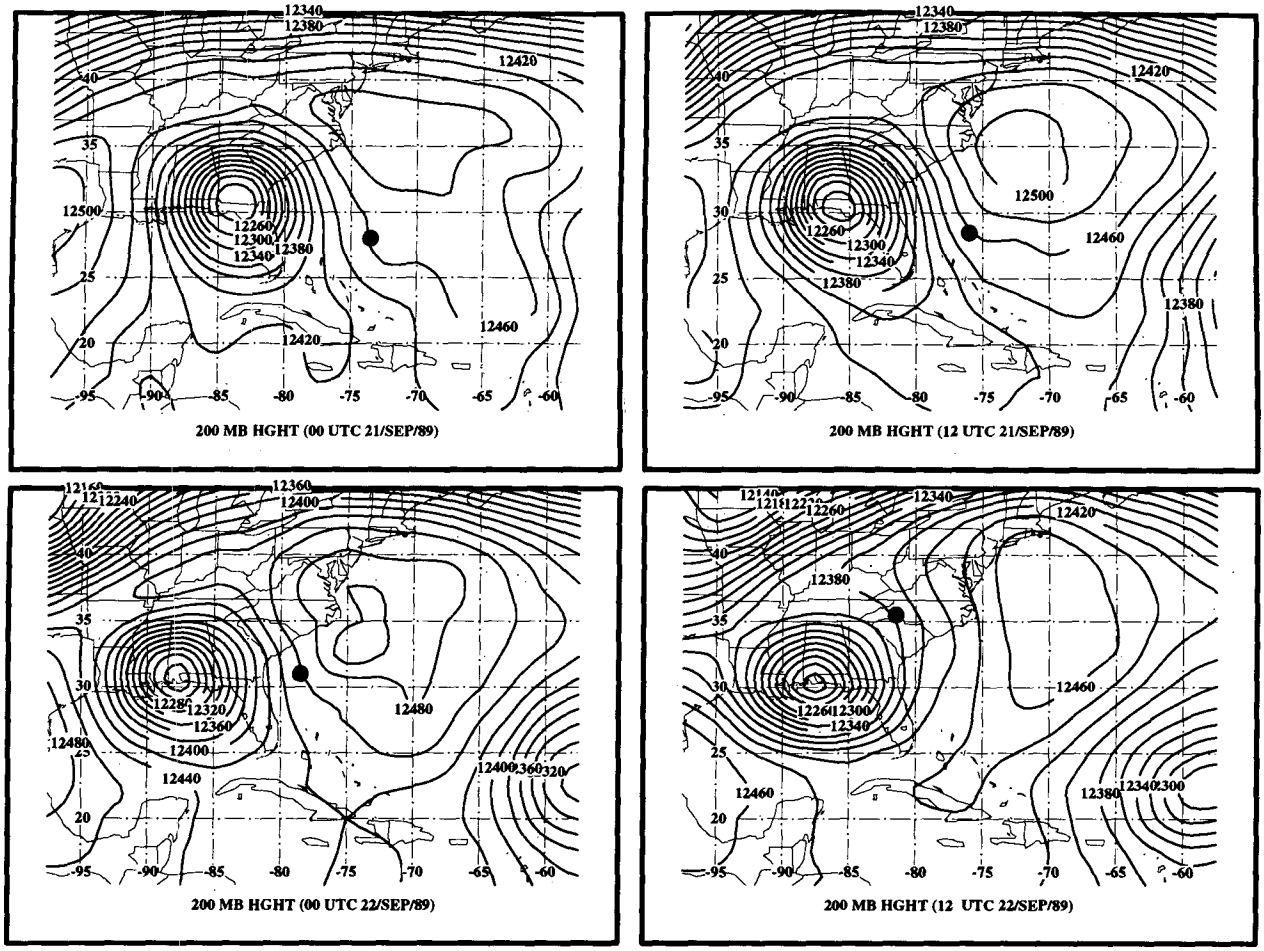

FIG. 13. ECMWF analysis of the western North Atlantic 200-mb geopotential heights (m) for 0000 and 1200 UTC for 21 and 22 September 1989. The dot represents Hugo's best-track position at the given times.

On 20 September, Hugo reintensified and reached its secondary maximum of less than 930 mb before it made landfall on 22 September near Charleston, South Carolina (Case and Mayfield 1990). Figure 14 delineates Hugo's best track during 10–22 September and the SSM/I observation times.

a. Hugo's latent heat release change versus intensity change

Although the spatial and temporal resolutions of the SSM/I observation are poor, Hugo's azimuthally mean inner-core LHR and minimum surface pressure observed in Fig. 15 suggested that there were three episodes of enhanced inner-core LHR. The first occurred on 12 September, the second on 16 September, and the third between 20 and 22 September. Since there were no SSM/I observations on 20 and 21 September, the timing and the magnitude of the third episode of enhanced inner-core LHR could not be ascertained. Even so, the periods of elevated mean LHR again appeared to precede times of intensification. For example, the period of rapid intensification that was initiated on 13 September appeared to follow the first episode of enhanced inner-core LHR. Likewise, the period of reintensification on 17 September followed the second episode of enhanced inner-core LHR. Finally, Hugo's period of reintensification prior to the South Carolina landfall followed the third episode of enhanced inner-core LHR. It is also noted that the magnitude of Hugo's maximum azimuthally mean inner-core LHR was larger than the maximum LHR observed in either Dean (see Fig. 4) or Gabrielle (see Fig. 9). Alliss et al. (1992) presents additional information concerning Hugo's latent heat distribution and its relationship with sequential periods of intensification.

b. The evolution of Hugo's precipitation

The radial distribution of Hugo's azimuthally averaged precipitation rates and maximum winds for the period between 10 and 22 September are seen in Fig.

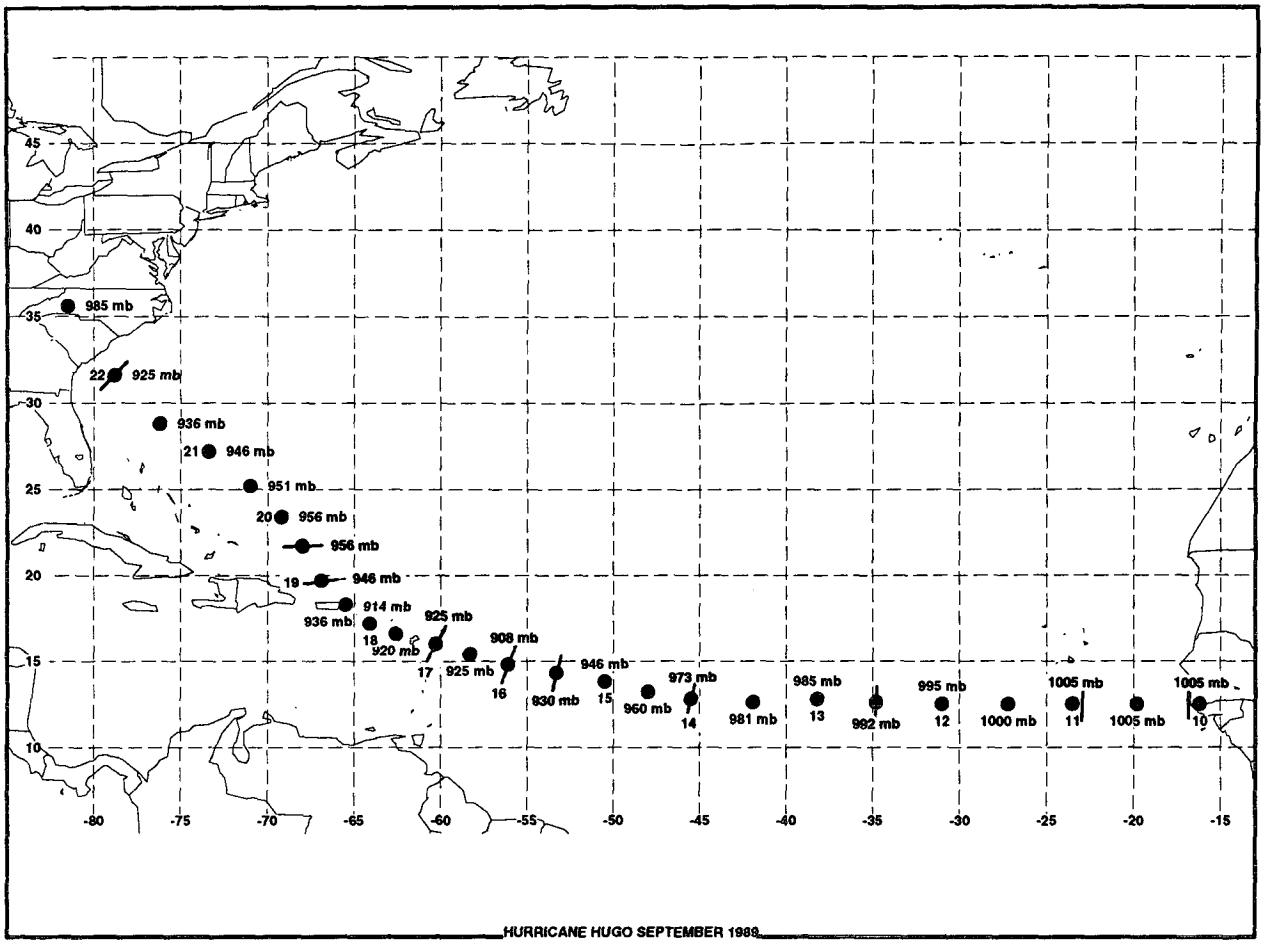

FIG. 14. The best-track positions and intensity of western Atlantic Tropical Cyclone Hugo (10–22 September 1989). Otherwise, similar to Fig. 3.

16. Even though the temporal and spatial resolutions of the SSM/I observation are poor, the figure again depicts convective ring cycles similar to those observed in Dean and Gabrielle. In this case, however, there appear to be four distinct convective rings that propagate inward (denoted, respectively, by heavy dashed lines 1, 2, 3, and 4 in the figure). The first convective ring originated in the annulus nearest the center on 10 September. Precipitation in this convective ring reached a maximum on 11 September, then rapidly decreased on 13 September. The second convective ring originated 165 km from the center on 10 September and propagated inward, reaching the inner annulus on 14 September. The third convective ring originated 222 km from the center on 15 September and propagated rapidly inward, reaching the innermost annulus on 17 September. This convective ring rapidly diminished on the following day. Finally, the fourth convective ring originated 222 km from the center on 16 September and propagated inward, reaching the innermost annulus on 22 September. It is interesting to note that as the outer convective rings came to within 55 km of the inner convective rings, the inner convective rings quickly dissipated, just as in Dean and Gabrielle.

The comparison between the evolution of Hugo's radial distribution of azimuthally averaged precipitation rates and maximum winds (Fig. 16) shows, as in Dean and Gabrielle, that the propagation of these convective rings to within 55 km of the center caused Hugo to intensify, while the dissipation of these convective rings caused Hugo to weaken. For example, the period of rapid intensification between 12 and 15 September appeared to be associated with the inward propagation of the second convective ring. As the second convective ring dissipated on 16 September, Hugo weakened. As the third convective ring propagated toward the center on 17 September, Hugo momentarily intensified before moving across the eastern edge of Puerto Rico. During this time Hugo weakened as the third convective ring dissipated. Between 20 September and prior to landfall on the South Carolina coast, Hugo again intensified as the fourth convective ring propagated toward the center.

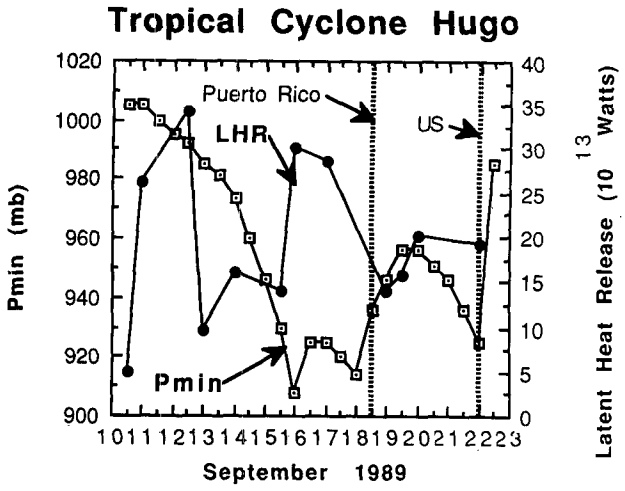

FIG. 15. A time plot of Hugo's minimum central pressure and the SSM/I-derived inner-core azimuthally averaged latent heat release. Otherwise, similar to Fig. 4.

It appears, once again, that the SSM/I can monitor tropical cyclone convective ring cycles and that these convective cycles are diverse. In the case of Hugo's convective cycles, the system had four convective ring cycles and each convective ring propagated toward the center, unlike Dean or Gabrielle. As in Dean and Gabrielle, intensification occurred when the convective rings formed and propagated inward to within 111 km of the center, while weakening was associated with the dissipation of these convective rings.

c. *External influences on Hugo's precipitation*

Figure 17 shows the external forcing mechanisms that influenced Hugo's convective ring cycles. The figure indicates that:

1) The SSTs that Hugo encountered increased slightly as Hugo moved westward. Between 18 and 20 September, Hugo reached maximum SSTs greater than 28°C that decreased to values less than 28°C prior to landfall on the South Carolina coast.

2) The vertical wind shear was nearly 10 m s^{-1} during 12, 16, 19, and 22 September. Maximum values were less than that observed with Dean and Gabrielle, however.

3) An inward flux of tropospheric moisture occurred throughout most of Hugo's life, except on 13 and 16 September. The maximum influx of moisture was concentrated mainly in the western half of the system prior to 19 September then shifted to the northeast quadrant as Hugo accelerated toward the South Carolina coast. There were two periods when Hugo experienced large inward surges of tropospheric moisture. The first occurred on 15 September and abruptly ended the next day. The second began on 17 September and continued until Hugo reached the South Carolina coast. On 20 September, however, the inward flux of tropospheric moisture momentarily decreased to about half of its original values, but rapidly increased prior to landfall. The maximum magnitude of the inward flux of tropospheric moisture was comparable to that experienced by Gabrielle, but less than that observed with Dean.

4) Hugo, unlike the first two tropical cyclones examined in this study, stayed in the low latitudes during its lifetime and never interacted with midlatitude upper-tropospheric troughs. Because of this lack of interaction, Hugo's upper-tropospheric ERFC was considerably less than that found with both Dean and Gabrielle. However, as Hugo began to interact with the upper-tropospheric closed low over the southeastern United States (see Fig. 15) prior to reaching the South Carolina coast, the upper-tropospheric closed low channeled and accelerated Hugo's outflow and enhanced the system's upper-tropospheric ERFC.

Comparison of the external forcing parameters observed in Fig. 17 with the convective ring cycles in Fig. 16 indicated that the initiation of the first two convective rings was probably caused by the enhanced inward flux of tropospheric moisture that occurred on 10 and 11 September as Hugo moved off the African coast into a region of warm SSTs and low vertical wind shear. Since Hugo had not reached hurricane stage before 11 September, the enhanced inward flux of tropospheric moisture may have reached Hugo's inner core and ini-

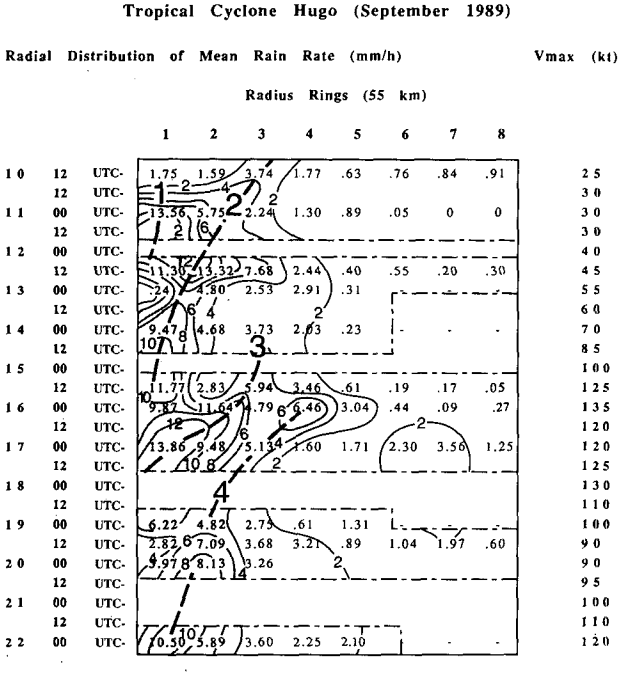

FIG. 16. The time change of Hugo's azimuthally averaged SSM/I-derived rain rates for annuli 1–8 and maximum wind speed. Otherwise, similar to Fig. 5.

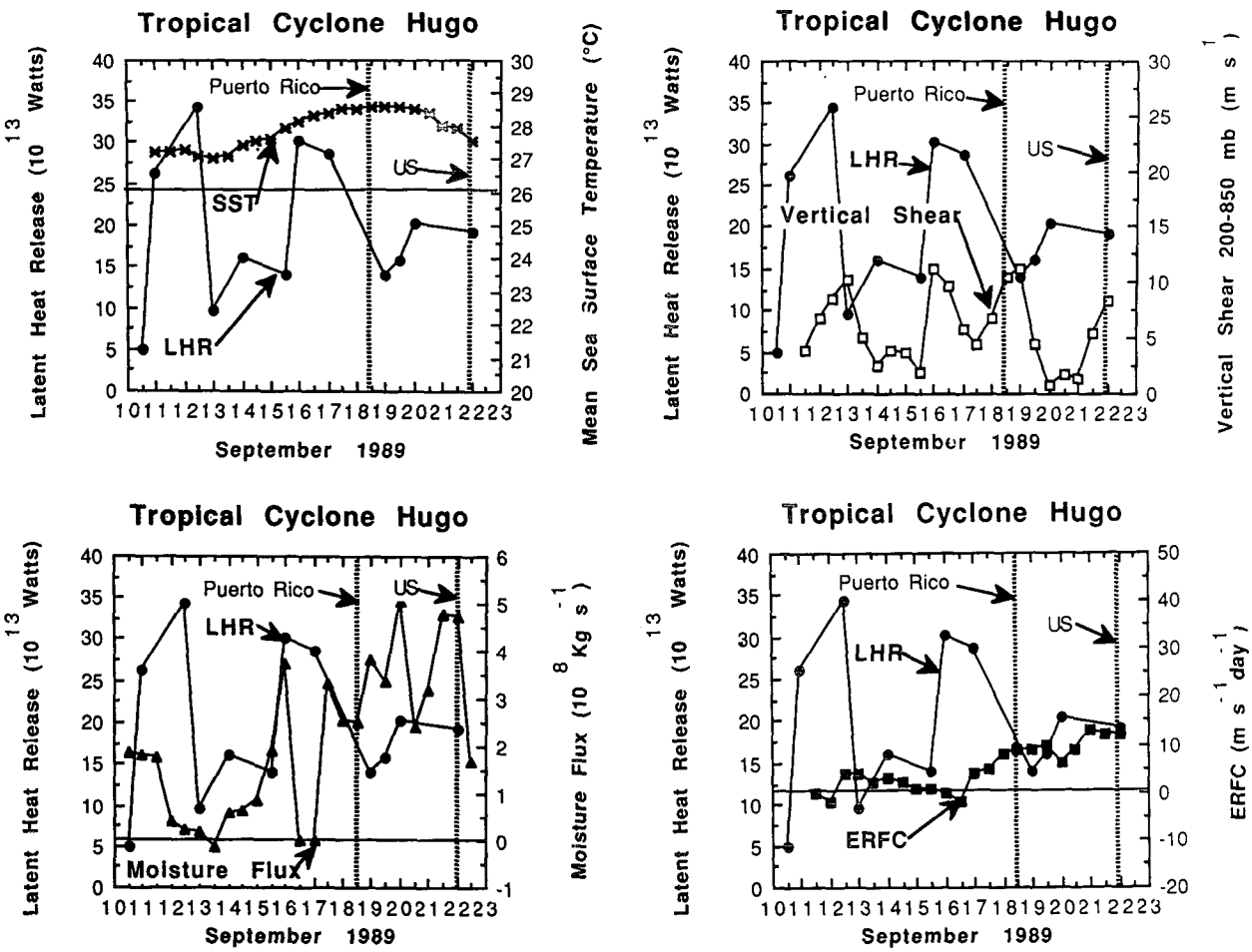

FIG. 17. A time plot of Hugo's inner-core SSM/I-derived azimuthally averaged latent heat release and the external forcing parameters. Otherwise, similar to Fig. 6.

tiated the first convective ring. As the second convective ring propagated inward to within 111 km of the center, it dissipated the first convective ring. On 12 and 13 September, the reduction in the precipitation in the second convective ring appeared to coincide with the increased vertical wind shear and the abrupt reduction in the influx of tropospheric moisture. During the following day, precipitation increased, once again, in possible response to the weaker vertical wind shear that Hugo encountered.

On 15 September, the third convective ring appeared to be initiated 165 km from the center by the large surge of tropospheric moisture that occurred when Hugo encountered SSTs near 28°C and low vertical wind shear. As this convective ring propagated inward into the inner core of Hugo on 16 September, the second convective ring quickly dissipated in response to the adverse effects of the third convective ring and the abrupt increase in the vertical wind shear.

The initiation of the fourth convective ring that formed 222 km from the center on 17 September appeared to coincide with the abrupt increase in the influx of tropospheric moisture. This convective ring quickly dissipated the third convective ring as it propagated toward the inner core on 18 September. After leaving Puerto Rico, Hurricane Hugo encountered warm SSTs ($\sim$28°C), weak vertical wind shear (<5 m s^{-1}), and the upper-tropospheric closed low over the southeastern United States that enhanced Hugo's ERFC. These ideal conditions may have caused the precipitation to reach a maximum before Hugo entered the South Carolina coast on 22 September. Although the influx of tropospheric moisture was ideal for enhancing precipitation in this convective ring, it is unlikely that it had any influence in enhancing the precipitation, since the convective ring was within the annulus nearest to the center where the lower-tropospheric inertial stability was strong.

Thus, it is once again apparent from this case study that the convective ring cycle can be identified and monitored in tropical cyclones using the SSM/I. These convective rings appeared to intensify Hugo as they

propagated toward the center and dissipated the preexisting inner convective ring. The rapid dissipation of these inner convective rings always initiated a period of weakening. It was also observed that in regions of warm SSTs (>26°C) and weak vertical shear (<10 m s^{-1}) the initiation and maintenance of convective rings outside the radius of maximum winds were controlled by inward surges of tropospheric moisture. Within the radius of maximum winds, however, where the lower-tropospheric inertial stability is large, the upper-tropospheric ERFC appeared to play a larger role in enhancing the precipitation.

8. Summary and conclusions

The SSM/I on board the DMSP F-8 was used to monitor the evolution of the precipitation in Hurricanes Dean, Gabrielle, and Hugo during 1989, while the VICBAR and ECMWF analyses helped to examine the relationship between the evolution of the precipitation in these tropical cyclones and external forcing. The forcing parameters examined were the mean climatological SSTs, vertical wind shear, tropospheric moisture flux, and upper-tropospheric eddy relative angular momentum flux convergence (ERFC).

Even though the SSM/I temporal and spatial resolution was poor, it was possible to delineate and monitor convective ring cycles that were similar to those observed from aircraft in situ measurements and by land-based and aircraft radar (Willoughby et al. 1982; Willoughby 1988, 1990). These convective rings usually formed in the outer core (e.g., 111–222 km from the center) and would last approximately 4–5 days as they propagated inward. An increase in precipitation and an inward propagation of these convective rings may have caused these tropical cyclones to intensify. The tropical cyclones appeared to reach their maximum intensity when their convective rings approached the center. Secondary convective rings, on the other hand, that formed outside the region of the original convective ring, appeared to dissipate the original convective ring by reducing its lateral inward flux of tropospheric moisture and subjecting the inner-core convective ring to subsiding dry air. The dissipation of the inner-core convective rings appeared to occur when the outer convective ring came to within 55 km of the original convective ring, causing the tropical cyclone to weaken.

In mature tropical cyclones located over ocean regions with SST $\geq$ 26°C and weak vertical wind shear (e.g., $\leq$5 m s^{-1}), initiation and maintenance of these convective rings outside the region of strong lower-tropospheric inertial stability appeared to be controlled by the strong influx of tropospheric moisture. On the other hand, strong influx of tropospheric moisture may have initiated and maintained the convective rings in weak tropical cyclones at all radii. Finally, the precipitation in the convective rings located in the inertially stable region of the mature tropical cyclone appeared to be enhanced by upper-tropospheric ERFC. However, since the upper-tropospheric troughs that increased their ERFC would also subject these systems to strong vertical shear, it was difficult to ascertain what influence the upper-tropospheric ERFC had in enhancing the precipitation rates in their inner-core convective rings.

Thus, these analyses suggest that in order to better understand tropical cyclone intensification process, it is important to monitor not only the external forcing mechanisms (De Maria et al. 1993), but to also relate external forcing to the convective ring cycle (Willoughby et al. 1982; Willoughby 1988, 1990). These analyses also suggest that convective ring cycles can be monitored from satellite-flown active and passive microwave radiometers when the systems are in the data-void ocean regions. When the populated land regions are being threatened by these tropical cyclones, however, these satellite observations should be augmented with higher temporal and spatial resolution radar observations when possible.

Acknowledgments. The authors would like to thank Dr. Robert Adler for providing support and valuable comments on this study and Dr. Mohan Karyampudi for his contribution.

REFERENCES

Adler, R. F., and E. B. Rodgers, 1977: Satellite-observed latent heat release in a tropical cyclone. *Mon. Wea. Rev.*, **105,** 956–963.

——, and A. J. Negri, 1993: An intercomparison of three satellite infrared rainfall techniques over Japan and surrounding waters. *J. Appl. Meteor.*, **32,** 357–373.

——, H-Y. M. Yeh, N. Prasad, W-K. Tao, and J. Simpson, 1991: Microwave simulations of a tropical rainfall system with a three-dimensional cloud model. *J. Appl. Meteor.*, **30,** 924–953.

——, A. J. Negri, P. R. Keenh, and I. M. Hakkarinen, 1993: Estimation of monthly rainfall over Japan and surrounding waters from a combination of low-orbit microwave and geosynchronous IR data. *J. Appl. Meteor.*, **32,** 335–356.

Alliss, R. J., S. Raman, and S. W. Chang, 1992: Special Sensor Microwave/Imager (SSM/I) observations of Hurricane Hugo. *Mon. Wea. Rev.*, **120,** 2723–2737.

Baik, J-J., 1989: Tropical cyclone simulations with the Betts convective adjustment scheme. Ph.D. dissertation, North Carolina University, 159 pp. [Available from North Carolina Univ., Raleigh, NC 27695.]

Black, P. G., and R. A. Anthes, 1971: On the asymmetric structure of the tropical cyclone outflow layer. *J. Atmos. Sci.*, **28,** 1348–1366.

Case, R. A., and M. Mayfield, 1990: Atlantic hurricane season of 1989. *Mon. Wea. Rev.*, **118,** 1165–1177.

Challa, M., and R. Pfeffer, 1980: Effects of eddy flux of angular momentum on model hurricane development. *J. Atmos. Sci.*, **37,** 1603–1618.

Charney, J. G., and A. Elliassen, 1964: On the growth of the hurricane depression. *J. Atmos. Sci.*, **21,** 68–75.

Chen, L., and W. M. Gray, 1985: Global view of the upper level outflow patterns associated with tropical cyclone intensity changes during FGGE. Colorado State University, Atmospheric Science Paper, 392, 1216 pp. [Available from Colorado State Univ., Fort Collins, CO 80523.]

Delden, A. van, 1989: On the deepening and filling of balanced cyclones by diabatic heating. *Meteor. Atmos. Phys.*, **41,** 127–145.

Demaria, M., J-J. Baik, J. Kaplan, 1993: Upper-level eddy angular momentum fluxes and tropical cyclone intensity change. *J. Atmos. Sci.*, **50,** 1133–1147.

Emanuel, K. A., 1986: An air–sea interaction theory for tropical cyclones. Part 1: Steady-state maintenance. *J. Atmos. Sci.*, **43,** 585–604.

Frank, W. M., 1977: The structure and energetics of the tropical cyclone. Part 1: Storm structure. *Mon. Wea. Rev.*, **105,** 1119–1135.

Gentry, R. C., E. Rodgers, J. Steranka, and W. Shenk, 1980: Predicting tropical cyclone intensity using satellite measured equivalent blackbody temperature of cloud tops. *Mon. Wea. Rev.*, **108,** 445–455.

Gray, W. M., 1979: Hurricanes: Their formation structure and likely role in the tropical circulation. *Meteorology over the Tropical Oceans.* D. B. Shaw, Ed., Roy. Meteor. Soc., 155–218.

——, and D. F. Shea, 1973: The hurricane inner core region. Part 2: Thermal stability and dynamic characteristics. *J. Atmos. Sci.*, **8,** 1565–1576.

——, and R. W. Jacobson, Jr., 1977: Diurnal variation of deep cumulus convection. *Mon. Wea. Rev.*, **105,** 1171–1188.

Hack, J. J., and W. H. Schubert, 1986: On nonlinear response of atmospheric vorticities to heating by organized cumulus convection. *J. Atmos. Sci.*, **45,** 1559–1573.

Holland, G. L., 1983: Angular momentum transport in tropical cyclones. *Quart. J. Roy. Meteor. Soc.*, **109,** 187–210.

——, and R. T. Merrill, 1984: On the dynamics of tropical cyclone structural changes. *Quart. J. Roy. Meteor. Soc.*, **110,** 723–745.

Huffman, G. J., R. F. Adler, P. R. Deehn, and A. J. Negri, 1993: Examples of global rain estimates from combined low-orbit microwave and geosynchronous IR data. *Proc. 4th Symp. Climate Change* Studies, Anaheim, CA, Amer. Meteor. Soc., 318–323.

Kurihara, Y., and R. E. Tuleya, 1974: Structure of a tropical cyclone developed in a three-dimensional numerical simulation model. *J. Atmos. Sci.*, **31,** 893–919.

Lee, C. S., 1986: An observational study of tropical cloud cluster evolution and cyclogenesis in the western North Pacific. Colorado State University, Atmospheric Science Paper 403, 250 pp. [Available from Colorado State Univ., Fort Collins, CO 80523.]

Levitus, S., 1982: *Climatological Atlas of the World Ocean.* NOAA Prof. Paper 13.

MacArthur, P. D., 1991: Microwave derived rain rates in typhoons and their use in the diagnosis and prediction of typhoon intensity. M.S. thesis, St. Louis Univ., 69 pp. [Available from St. Louis Univ., St. Louis, MO 63103.]

Merrill, R. T., 1984: Structure of the tropical cyclone outflow layer. Preprints, *15th Conf. Hurricanes and Tropical Meteorology,* Miami, FL, Amer. Meteor. Soc., 421–426.

——, 1988: Environmental influence on hurricane intensification. *J. Atmos. Sci.*, **45,** 1678–1687.

Molinari, J., and S. Skubis, 1985: Evolution of the surface wind field in an intensifying tropical cyclone. *J. Atmos. Sci.*, **42,** 2865–2879.

——, and D. Vollaro, 1989: External influences on hurricane intensity. Part 1: Outflow layer eddy momentum fluxes. *J. Atmos. Sci.*, **46,** 1093–1105.

Mundell, D. B., 1991: Tropical cyclone intensification. Preprints, *19th Conf. Hurricanes and Tropical Meteorology,* Miami, FL, Amer. Meteor. Soc., 511–515.

Ooyama, K. V., 1964: A dynamical model for the study of tropical cyclone development. *Geifus, Int.*, **4,** 187–198.

——, 1987: Scale-controlled objective analysis. *Mon. Wea. Rev.*, **115,** 2479–2506.

Palmén, E., and H. Riehl, 1957: Budget of angular momentum and energy in tropical cyclones. *J. Meteor.*, **14,** 150–159.

Pfeffer, R. L., 1958: Concerning the mechanisms of hurricanes. *J. Meteor.*, **15,** 113–119.

Reed, R. J., A. Hollingsworth, W. A. Heckley, and F. Delsol, 1988: An evaluation of the performance of the ECMWF operational system in analyzing and forecasting easterly wave disturbances over Africa and the tropical Atlantic. *Mon. Wea. Rev.*, **116,** 824–865.

Riehl, H., and J. S. Malkus, 1961: Some aspects of Hurricane Daisy, 1958. *Tellus,* **13,** 181–213.

Rodgers, E. B., and R. F. Adler, 1981: Tropical cyclone rainfall characteristics as determined from a satellite passive microwave radiometer. *Mon. Wea. Rev.*, **109,** 506–521.

——, S. W. Chang, J. Stout, J. Steranka, and J-J. Shi, 1991: Satellite observations of variations in tropical cyclone convection caused by upper-tropospheric troughs. *J. Appl. Meteor.*, **30,** 1163–1184.

Rosenthal, L., 1978: Numerical simulation of tropical cyclone development with latent heat release by the resolvable scales. Part 1: Model description and preliminary results. *J. Atmos. Sci.*, **35,** 258–271.

Reuter, G. W., and M. K. Yau, 1986: Numerical modeling of cloud development in a shear environment. *Beitr. Phys. Atmos.*, **60,** 65–80.

Sadler, J. C., 1976: Tropical cyclone initiation by the tropical upper-tropospheric trough. *Mon. Wea. Rev.*, **104,** 1266–1278.

——, 1978: Midseason typhoon development and intensity changes and the tropical upper-tropospheric trough. *Mon. Wea. Rev.*, **106,** 1137–1152.

Schubert, W. H., and J. J. Hack, 1982: Inertial stability and tropical cyclone development. *J. Atmos. Sci.*, **39,** 1687–1697.

Shapiro, L. J., and H. E. Willoughby, 1982: The response of balanced hurricanes to local sources of heat and momentum. *J. Atmos. Sci.*, **39,** 378–394.

Shaw, D. B., P. Lonnberg, A. Hollingsworth, and P. Unden, 1987: Data assimilation: The 1984/1985 revisions of the ECMWF mass and wind analysis. *Quart. J. Roy. Meteor. Soc.*, **113,** 533–566.

Shenk, W. E., H. Powell, V. V. Salomonson, and W. R. Bandeen, 1971: Meteorological uses of the stereographic horizon map projection. *J. Appl. Meteor.*, **110,** 582–589.

Shi, J-J., S. W. Chang, and S. Raman, 1990: A numerical study of the outflow layer of tropical cyclones. *Mon. Wea. Rev.*, **118,** 2042–2055.

Steranka, J. E., E. B. Rodgers, and R. C. Gentry, 1984: The diurnal variation of Atlantic Ocean tropical cyclone cloud distribution inferred from geostationary satellite infrared measurements. *Mon. Wea. Rev.*, **112,** 2338–2344.

——, ——, and ——, 1986: The relationship between satellite-measured convective burst and tropical cyclone intensification. *Mon. Wea. Rev.*, **114,** 1539–1546.

Velden, C. S., W. S. Olson, and B. A. Roth, 1989: Tropical cyclone center-fixing using SSM/I data. Preprints, *18th Conf. on Hurricanes and Tropical Meteorology,* San Diego, CA, Amer. Meteor. Soc., J36–J39.

Weatherford, C., 1987: Typhoon structural evolution. Preprints, *17th Conf. on Hurricanes and Tropical Meteorology,* Miami, FL, Amer. Meteor. Soc., 337–340.

Willoughby, H. E., 1988: The dynamics of the tropical cyclone core. *Aust. Meteor. Mag.*, **36,** 183–191.

——, 1990: Temporal changes of the primary circulation in tropical cyclones. *J. Atmos. Sci.*, **47,** 242–264.

——, J. A. Clos, and M. G. Shoreibah, 1982: Concentric eyewalls, secondary wind maxima, and the evolution of the hurricane vortex. *J. Atmos. Sci.*, **39,** 395–411.

Zehr, R. M., 1988: Satellite diagnostics of tropical cyclones. Preprints, *Third Conf. on Satellite Meteorology and Oceanography,* Anaheim, CA, Amer. Meteor. Soc., 241–246.

——, 1992: Tropical cyclogenesis in the western North Pacific. NOAA Tech. Report NESDIS 61, 181 pp.